January 2017

Sensitivity Of Cross-Tropopause Convective Transport To Tropopause Definition

Emily Maddox

Follow this and additional works at: https://commons.und.edu/theses

SENSITIVITY OF CROSS-TROPOPAUSE CONVECTIVE TRANSPORT TO TROPOPAUSE DEFINITION

by

Emily M. Maddox
Bachelor of Science, University of North Dakota, 2015

A Thesis

Submitted to the Graduate Faculty

of the

University of North Dakota

in partial fulfillment of the requirements

for the degree of

Master of Science

Grand Forks, North Dakota
August
2017

This thesis, submitted by Emily M. Maddox in partial fulfillment of the requirements for the Degree of Master of Science from the University of North Dakota, has been read by the Faculty Advisory Committee under whom the work has been done and is hereby approved.

_____
Dr. Gretchen Mullendore

_____
Dr. Baike Xi

_____
Dr. Cameron Homeyer

This thesis is being submitted by the appointed advisory committee as having met all of the requirements of the School of Graduate Studies at the University of North Dakota and is hereby approved.

_____
Grant McGimpsey
Dean of the School of Graduate Studies

_____
DATE

PERMISSION

Title	Sensitivity of Cross-Tropopause Convective Transport to Tropopause Definition
Department	Atmospheric Sciences
Degree	Master of Science

In presenting this thesis in partial fulfillment of the requirements for a graduate degree from the University of North Dakota, I agree that the library of this University shall make it freely available for inspection. I further agree that permission for extensive copying for scholarly purposes may be granted by the professor who supervised my thesis work or, in her absence, by the Chairperson of the department or the dean of the School of Graduate Studies. It is understood that any copying or publication or other use of this thesis or part thereof for financial gain shall not be allowed without my written permission. It is also understood that due recognition shall be given to me and to the University of North Dakota in any scholarly use which may be made of any material in my thesis.

Emily M. Maddox
July 30, 2017

TABLE OF CONTENTS

LIST OF TABLES

ACKNOWLEDGMENTS

I dedicate this thesis to my father, Randy. Without you, I never would have gotten over my fear of thunderstorms, found a passion for meteorology, or had the courage to continue reaching for my goals when Carl was against me.

ABSTRACT

An idealized three-dimensional cloud–resolving model is used to investigate the sensitivity of cross–tropopause convective mass transport to tropopause definition. A ten–hour simulation is conducted to encompass the growth and decay cycle, with focus on irreversible transport above the tropopause. Six previously published tropopause definitions are evaluated. These definitions include specific values of altitude, World Meteorological Organization (WMO) temperature lapse rate, potential vorticity, stratospheric tracer concentration, static stability, and curvature of the Brunt–Väisälä Frequency. This investigation highlights the challenge of defining a tropopause during active deep convection, and demonstrates the need of clearly communicating calculation methods and threshold choices in the literature. Definitions such as potential vorticity and stratospheric tracer are shown to perform poorly when analyzing deep convection. The WMO thermal tropopause and static stability tropopause definitions perform the best, providing similar tropopause placement and quantities of irreversible mass transport.

An additional small investigation of the universality of tropopause definitions, including the WMO and static stability definitions, between the midlatitudes and tropics is performed using the Weather Research and Forecasting model. First, a thought experiment demonstrates that the WMO thermal tropopause identifies areas of similar temperature lapse rates, not necessarily similar stability, which plays an important role in mass transport. To investigate further, two case studies are analyzed to determine the tropopause placement in each region. Again, the WMO and static stability definitions provide similar placement of the tropopause in both regions.

CHAPTER 1

INTRODUCTION

The chemical budget and radiative balance in the upper troposphere and lower stratosphere (UTLS) are greatly influenced by the transport of chemical constituents from the boundary layer to the stratosphere (*Dickerson et al.*, 1987; *Hauf et al.*, 1995; *Santer et al.*, 2003; *Skamarock et al.*, 2000; *Twohy et al.*, 2002). These chemical constituents include greenhouse gases such as water vapor, carbon dioxide, and ozone. Although large–scale stratosphere–troposphere exchange (STE) is understood fairly well, small-scale transport, such as that occurring through deep convection, has not been thoroughly examined. Deep convection is important to STE because it efficiently transports air from the boundary layer to the stratosphere (*Dickerson et al.*, 1987; *Feichter and Crutzen*, 2002; *Fischer et al.*, 2003; *Hauf et al.*, 1995; *Poulida et al.*, 1996). These boundary layer tracers can be deposited in the lower stratosphere if heated enough to become neutrally buoyant. This heating can occur through a variety of methods such as latent heating of an air parcel and turbulent mixing at the cloud top (*Mullendore et al.*, 2005). To further understand STE, we must be able to quantify tropopause structure and variability (*Randel et al.*, 2007). To quantify the tropopause structure and variability, we must have an appropriate tropopause definition. An incorrect tropopause placement could result in an overestimate or underestimate of mass transport from the troposphere to the lower stratosphere. Therefore, it is important to have a definition that properly places the tropopause during and after a convective event. Having multiple definitions that provide similar results continues

1

to provide freedom of using definitions best suited for a study, while still allowing readers to compare results between mass transport studies.

Observations of winds, temperature, and trace gases suggest the transition from the troposphere to the stratosphere occurs over a finite depth rather than a single point transition *Fueglistaler et al.* (2009). In the tropics, this broad layer is commonly referred to as the "tropical tropopause layer" or the "tropical transition layer" (TTL). However, in this study tropopause altitudes are treated as boundaries rather than layers. Several tropopause definitions exist in the current literature and can be broken up into six main categories: constant altitude, temperature lapse rate, cold point temperature, potential vorticity iso–surfaces, static stability iso–surfaces, and trace gas–based. Constant altitude tropopause definitions are appropriate only in an idealized model framework. Temperature lapse rate tropopause definitions include the World Meteorological Organization (WMO) thermal tropopause (*WMO*, 1957). Cold point temperature tropopause definitions are applicable only in the tropics. Potential Vorticity (PV) tropopause definitions apply only to the extratropics and on syntopic scales (*Gettelman et al.*, 2011). Static stability definitions include vertical gradient thresholds, such as that used in *Mullendore et al.* (2005) and the maximum vertical curvature of the Brunt–Väisälä frequency (BVF) (*Birner*, 2010). Lastly, trace gas tropopause definitions, also known as chemical tropopauses, include ozone lapse rates and tracer–tracer relationships (*Bethan et al.*, 1996; *Zahn et al.*, 2004). This study will analyze six tropopause definitions in five categories: a constant altitude, the WMO thermal tropopause, PV, stratospheric tracer, static stability, and the maximum curvature of the BVF. Each definition is described in further detail in sections 2.4 and 3.2.

Convective systems such as supercells efficiently transport boundary layer tracers, providing deeper injection of lower tropospheric tracers into the lower strato-

sphere. *Mullendore et al.* (2005) found greater amounts of boundary layer tracer transported to the lower stratosphere in supercell cases compared to multicell cases. Therefore, this study will analyze the sensitivity of mass transport to tropopause definition in a simulated midlatitude supercell storm in a controlled environment. Section 2.2 discusses the methods of transport and previous studies highlighting the importance of deep convective transport. A basic description of supercellular convection is provided in section 2.3. The transport results from the idealized supercell simulation are presented in chapter 4. Tropopause definitions in a model simulation of an observed event, comparing midlatitude to tropical environments, are presented in chapter 5.

CHAPTER 2

BACKGROUND

To understand the sensitivity of mass transport to tropopause definition, we must first understand the tropopause region and the types of definitions that will be analyzed. The tropopause definition has an impact on mass transport, altering the exact height of the tropopause. This section provides an overview of the current understanding of tropopause structure and the varying definitions used to define the extratropical upper troposphere and lower stratosphere (Ex-UTLS).

2.1   The Discovery of the Tropopause

In 1787 Horace Benedict de Saussure climbed Mont Blanc with a thermometer and barometer to determine the vertical profile of the atmosphere (*Hoinka*, 1997). He determined the temperature decreased at a rate of 0.7 K per 100 m. It was assumed that the temperature continued to decrease at that rate throughout the atmosphere, reaching a temperature of absolute zero at approximately 30 km.

In the following years, many individuals began investigating the vertical profile of the atmosphere using hot air balloons. These studies were limited to approximately 10 km due to the lack of oxygen at those studies. Sounding balloons were introduced in 1892 and a transition from use of hot air balloons to sounding balloons began. Using sounding balloons would allow measurements to be taken at higher altitudes. The use of sounding balloons was limiting, though, because the instruments used on them had large errors. The first high–level sounding balloon flight was conducted by Hermite

and Besancon on 21 March, 1893. At this time, the atmospheric temperature was still assumed to continuously decrease with height. Hermite and Besancon recorded a temperature of -21°C at 14.7 km. However, since the temperature recorded at 12.5 km was -51°C, they assumed their observation was erroneous.

Sounding balloon materials and tracking techniques began to improve throughout the following years. Instruments such as the aspirated thermometer were introduced which reduced instrument error, but still an isothermal layer was found by several individuals. This layer was still thought to be an instrument error and was often 'corrected' so the temperature continued to decrease with height, or was not discussed in results.

The stratosphere wasn't officially recognized in published papers until *Teisserenc de Bort* (1902) who presented the results of 236 soundings. He noted an isothermal zone which varies in a starting height from 8–12 km (*Hoinka*, 1997). Later in 1902, Dr. Robert Assmann confirmed the results of Teisserenc de Bort in a presentation to the Berlin Academy of Sciences. It is thought that Teisserenc de Bort coined the term "stratosphere" during the German Meteorological Society conference at Hamburn in September 1908 (*Kassner*, 1909). He chose this term because this nearly–isothermal layer has greater hydrostatic stability, suggesting it is stratified as opposed to mixed. He also suggested "troposphere" for the underlying atmosphere, where *tropos* means to turn in Greek.

The tropopause was later defined using thermal properties by the British Meteorological Office (*Hoinka*, 1997). *Hoinka* (1997) states three transition types were noted to classify the transition between the troposphere and stratosphere:

Type I: When the stratosphere commences with an inversion, the height of the tropopause is the first point of zero temperature gradient.

Type II: When the stratosphere begins with an abrupt transition to a temperature gradient below 2 K per km without inversion, the height of the tropopause is the height of the abrupt transition.

Type III: Where there is no such abrupt change in temperature gradient, the base of the stratosphere is to be taken at any point where the mean fall of temperature for the kilometer next above is 2 K or less, provided that it does not exceed 2 K for any subsequent kilometer.

In these criteria, the lapse rate, $\Gamma = -\frac{\Delta T}{\Delta z}$, is a decrease in temperature of 2 K km^{-1}.

This was later used by *WMO* (1957) to create the common thermal tropopause definition used today. This definition uses two criteria, where the tropopause is defined as "the lowest level at which the lapse rate decreases to 2 K km^{-1} or less, provided also the average lapse rate between this level and all higher levels within 2 km does not exceed 2 K km^{-1}" (*WMO*, 1957).

2.2 Extratropical Deep Convective Transport

Boundary layer tracers can be transported to the lower stratosphere in the extratropics through processes such as deep convection. Updrafts in deep convective storms are capable of injecting tropospheric tracers several kilometers into the lower stratosphere during a deep convective event. Tracers can be transported from the boundary layer to the lower stratosphere often within one hour (*Dickerson et al.*, 1987; *Feichter and Crutzen*, 2002; *Fischer et al.*, 2003; *Mullendore et al.*, 2005). Because this rapid transfer occurs, considerable vertical mixing occurs during isolated events such as supercells. According to *Fischer et al.* (2003), budget estimates suggest that lower stratospheric air could contain up to 50% boundary layer air during a deep convective event. However, the parcels remain negatively buoyant unless they

6

undergo processes such as latent heating in the updraft core and turbulent mixing at the cloud tops. These processes can increase the potential temperature of the tropospheric parcels enough to make them neutrally buoyant in the lower stratosphere. While extratropical deep convective transport is not considered to be the dominant method of transport of boundary layer tracers to the lower stratosphere, its efficiency in transporting tracers has been increasingly studied throughout the past few decades. The transport of chemical constituents such as water vapor into the lower stratosphere can increase cloud production, impacting the weather and climate. The influence of deep convection on tracer transport to the lower stratosphere was first observed during the early 1970s (*Fischer et al.*, 2003). Deep convective storms are capable of introducing significant amounts of water vapor into the lower stratosphere during a deep convective event (*Fischer et al.*, 2003). Additional studies (*Dickerson et al.*, 1987; *Hauf et al.*, 1995; *Skamarock et al.*, 2000) performed in the 1980s–2000s presented further evidence for STE of other tracers such as O_3 and CO.

To focus on irreversible transport, though, tracer plumes must be evaluated after a convective event and model simulations must include sufficient time to allow the environment to return to a non–convective state. During a convective event, the quantity of boundary layer tracer that is injected into the lowermost stratosphere does not equate to the quantity that will remain in the lowermost stratosphere after convection has dissipated. As stated before, some of the parcels are not immediately neutrally buoyant in the lowermost stratosphere. Therefore, many boundary layer parcels that are injected into the lowermost stratosphere return to the troposphere. To determine how tracer transport in deep convection impacts the weather and climate, the quantity of boundary layer tracer remaining in the lower stratosphere after a convective event must be studied. *Mullendore et al.* (2005) simulated the transport of boundary layer tracers into the lowermost stratosphere via midlatitude convection in a three–

dimensional cloud–resolving model. Ten–hour simulations were performed to ensure the model returned to a non–convective state in order to evaluate irreversible transport associated with three deep convective events. Air parcels containing boundary layer tracers were shown to penetrate the stable stratosphere via the updraft where diabatic processes increased the parcel potential temperature sufficiently to allow the parcel to become stable in the stratosphere. The results of *Mullendore et al.* (2005) showed irreversible transport for both multicell and supercell cases, where the supercell case transported nearly twice as much boundary layer tracer as the multicell case at ten hours.

2.3 Supercellular Convection

Supercells are classified as large, rotating thunderstorms that can last for several hours (*Markowski and Richardson*, 2012; *Lin*, 2010). They are associated with large hail (hail having a diameter of 5 cm or longer), high lightning flash rates, and strong, violent tornadoes (although tornadoes are not required for a storm to be classified as a supercell). Supercells are found in environments with strong vertical wind shear. This vertical wind shear generally extends throughout much of the troposphere and promotes storm organization and longevity. The longevity of a supercell can be promoted through dynamical vertical pressure gradients and its assistance to updraft intensification (*Markowski and Richardson*, 2012). Dynamic vertical pressure gradients are associated with environments with strong vertical wind shear. This can enhance the updraft at altitudes above the gust front, helping to sustain the storm. The enhancement of the updraft by the vertical wind shear is one aspect of supercells that sets them apart from other storm types whose updraft is mostly driven by buoyancy. Additionally, vertical wind shear helps prevent precipitation loading in the updraft. Environmental horizontal vorticity, or the horizontal vorticity already

present in the atmosphere, is tilted into the vertical by the storm. This process continues throughout the storm's active period as the moving updraft of the storm is the tilting mechanism. As the updraft intensifies, vorticity that has been vertically tilted is stretched, amplifying the updraft.

2.4   Tropopause Definitions

The Ex–UTLS, or the uppermost troposphere and lowermost stratosphere poleward of the subtropical jet (*Gettelman et al.* (2011); dark and light blue shading in figure 1), is bounded vertically by the stratospheric overworld (440 K isentropes) and the upper troposphere (about 5 km below the mean tropopause). This study focuses on irreversible transport to the lower stratosphere, whose lower bound is defined through the tropopause placement. Clearly seen in figure 1, the thermal tropopause (given by the black dots) and the potential vorticity tropopause (given by the light blue line) do not place the tropopause at the same altitude in all locations. Since the depth of the lower stratosphere depends on the altitude of the tropopause, its placement becomes very important when discussing transport to the lower stratosphere, as it has a direct impact on the amount of mass transported.

To be able to quantify irreversible transport of boundary layer tracers to the lower stratosphere in supercells, the tropopause must be mathematically defined. In the years after the tropopause was officially recognized, the thermal tropopause and the dynamical PV tropopause were the only definitions used. As more advanced studies were able to be conducted and improvements were made to study the vertical profile of the atmosphere, several more definitions were added to investigate the tropopause using different methods. Typically the tropopause definition is chosen to fit the study. Most studies investigate at most two tropopause definitions. To determine how applicable each definition is to convective transport, we must analyze
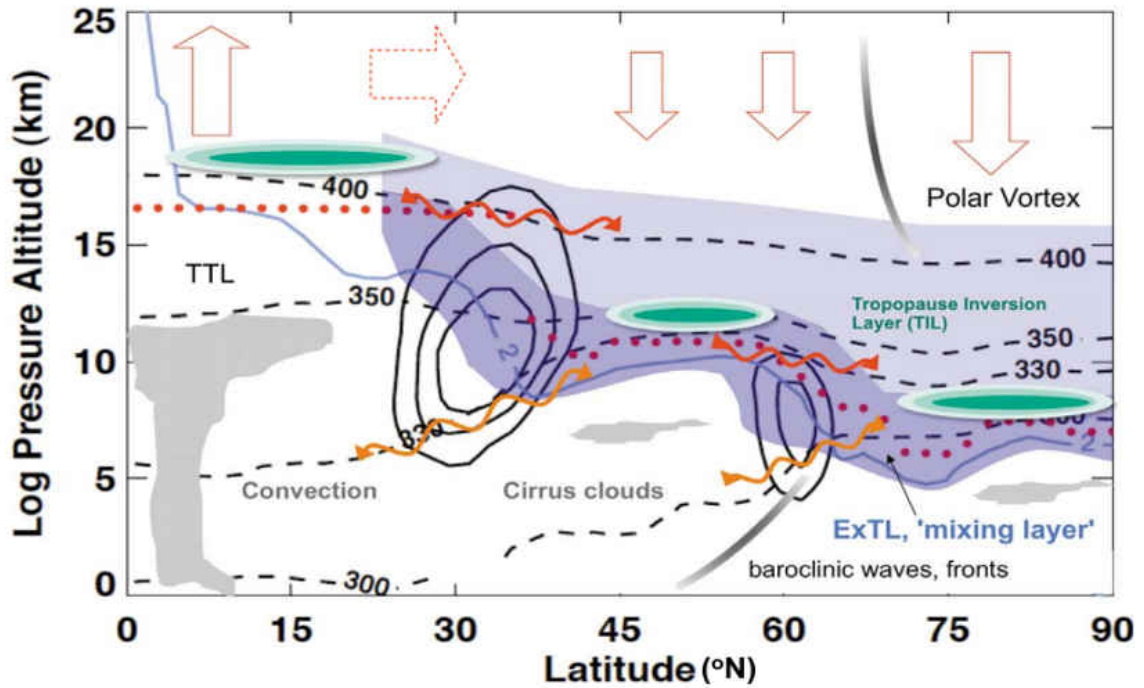
Figure 1: Schematic of the extratropical upper troposphere and lower stratosphere (Ex–UTLS) using data from a Northern Hemisphere section along 60∘W longitude on 15 February 2006. Wind contours (solid black lines 10 m s^{-1} interval), potential temperature surfaces (dashed black lines), thermal tropopause (red dots), and potential vorticity surface (2 potential vorticity unit (PVU): light blue solid line). Illustrated schematically are the Ex-UTLS (dark and light blue shading), extratropical tropopause layer (dark blue shading), clouds and fronts (gray shading), static stability contours in the tropopause inversion layer (green shading), quasi–isentropic exchange (red wavy arrows), cross–isentropic exchange (orange wavy arrows), and the Brewer–Dobson Circulation (deep, red solid outline arrows; shallow, dotted solid outline arrows). (*Gettelman et al.*, 2011).

several definitions. As mentioned before, six definitions were analyzed in this study: constant altitude, WMO, PV, stratospheric tracer, static stability, and curvature of the BVF. In this section, an overview of each definition is provided. Additional details on calculation method and equations used for each definition is provided in section 3.2.

2.4.1 Constant Altitude Tropopause

The constant altitude tropopause definition is only appropriate in an idealized framework. This definition does not adjust to convective perturbations, skewing results during active convection. However, this definition is still applicable to this study because the focus is on mass transport after convection has dissipated. After all convection has dissipated, tropopause altitudes generally return to a similar height to that prior to convection, where the tropopause location varies by only a few hundred meters throughout the domain.

2.4.2 WMO Tropopause

The WMO thermal tropopause definition uses two general criteria which allows it to identify the tropopause in a variety of thermal structures (*WMO*, 1957). The tropopause is defined as the lowest altitude at which the lapse rate has decreased to 2 K km^{-1}. As described in section 2.1, the thermal tropopause definition was the first definition used to identify the tropopause. This definition is widely used in studies and is the basic definition taught in meteorology classes. This definition continues to be used because the thermal structure is similar at all latitudes.

2.4.3 PV Tropopause

The potential vorticity dynamical tropopause definition, a common definition for synoptic–scale events or climatological studies in the extratropics, uses a subjectively chosen threshold value to determine the tropopause height (*Gettelman et al.*, 2011). The definition requires three–dimensional temperature and wind data, making it effective at determining the tropopause height in global models. The definition uses both static stability and vorticity (*Gettelman et al.*, 2011; *Kunz et al.*, 2011). PV is a conserved quantity for adiabatic, frictionless flow (*Holton*, 2013). Similarly to the Brunt–Väisälä Frequency, PV has an abrupt jump in values at the tropopause. This sharp change provides a useful dynamical definition for areas or model runs dominated by environmental vorticity.

When performing synoptic–scale studies, a 2 potential vorticity unit (PVU) surface, where $1PVU = 10^{-6}Km^2kg^{-1}s^{-1}$, is often chosen to represent the tropopause (*Kunz et al.*, 2011). However, this value is subject to change based on the study as the PVU surface should be chosen to represent the WMO thermal tropopause. For example, *Hoerling et al.* (1991) found that a 3.5 PVU isoline was optimal for their tropopause analysis because it statistically agreed with the thermal tropopause. *Kunz et al.* (2011) found a seasonal variation between 1.5 and 5 PVU in both the southern and northern hemispheres, with higher values during the summer and lower values during the winter. Although large variations in PVU values were found throughout the year, they agreed that overall a 2 PVU isoline represented the dynamical tropopause well.

2.4.4 Stratospheric Tracer Tropopause

The stratospheric tracer tropopause, also known as a chemical tropopause, is defined using a trace gas in the stratosphere (*Pan et al.* , 2004; *Zahn et al.*,

2004). The ozone mixing ratio is commonly used for the chemical tropopause, but determing the proper threshold value to use can be challenging. Some studies such as *Zahn et al.* (2004) use multiple trace gases with sources in both the troposphere and stratosphere to determine the tropopause. In their study, ozone, which has higher concentrations in the stratosphere, and carbon monoxide, which has higher concentrations in the troposphere, were used to determine the tropopause height from in–situ measurements. In this study a passive tracer, initially defined only in the stratosphere, was used.

2.4.5   Static Stability Tropopause

When analyzing mass transport, the stability of air parcels plays a vital role. In convective transport, the surface air parcels are transported to the UTLS, and unless heated, are negatively buoyant at those altitudes. The parcels must undergo heating processes to make them neutrally buoyant in the UTLS, creating irreversible transport. As stated earlier, these processes include latent heating, which dominates in the updraft core and can raise the parcel temperature several Kelvin, and turbulent mixing at the cloud top, which occurs through gravity wave breaking and mixing with stratospheric air to heat the parcel to remain neutrally buoyant.

The static stability tropopause is defined using the vertical gradient in potential temperature, where it is assumed $\frac{\partial \theta}{\partial z} = \frac{\Delta \theta}{\Delta z}$ in this study. This term is included in the equation used in the PV definition, the last term in equation 3.2 in section 3.2.2. Similarly to how the temperature lapse rate shows a distinct change between the troposphere and stratosphere, the potential temperature lapse rate also has a distinct change between the two layers. The troposphere is less stable than the stratosphere, where potential temperature increases faster with height in the stratosphere. In this study, the average potential temperature lapse rate in the troposphere was 0.003 K

m^{-1} while the average potential temperature lapse rate in the stratosphere was 0.018 K m^{-1}. This is clear by looking at the isentropes (thin horizontal lines) in figure 10 where the spacing between the isentropes decreases above 10.85 km at 0 hours.

The static stability definition uses a stability gradient which is most representative of the constant altitude tropopause in the pre–convective environment. *Mullendore et al.* (2005) states that it seems likely that air that is carried across a boundary with a strong stability gradient will likely remain lofted long enough to undergo mesoscale mixing, causing boundary layer air parcels to become neutrally buoyant in the lower stratosphere. In this study, a threshold value of 0.012 K m^{-1} was used. However, the threshold value is specific to each convective event simulated. For example, *Mullendore et al.* (2005) used a threshold of 0.00935 K m^{-1} to represent the tropopause. Throughout the storm's life cycle, the static stability definition often behaves similarly to the WMO definition, providing a realistic tropopause location during the active cycle and returning to a quasihorizontal state after all convection has dissipated.

2.4.6   Curvature of the Brunt–Väisälä Frequency Tropopause

The curvature of the BVF tropopause definition defines the tropopause through the curvature of the static stability in a column. The troposphere and stratosphere can be characterized by differences in their static stability, with the stratosphere being more stable. For an unperturbed atmosphere, *Birner* (2010) states that using the maximum vertical curvature of the BVF produces similar results to the standard WMO definition in the extratropics. It should be noted that this definition was intended for climate studies, not convection. This definition was included because when evaluating mass transport, the stability of an air parcel determines where it remains

14

after convection has dissipated. Unlike the static stability tropopause definition, this definition uses the maximum curvature of static stability.

CHAPTER 3

METHODOLOGY

3.1 University of Washington's Collaborative Model for Mesoscale Atmospheric Simulation (UWCOMMAS)

The model used to simulate the supercell used in this study was created by the University of Washington, referred to as *UWCOMMAS* in this study. The version of the model used in this study can be found by going to:

https://brume.atmos.washington.edu/svn/meso12. It should be noted that the model provided at this link does not include the modifications for the domain used in this study.

3.1.1 Numerics and Case Description

This study used a three–dimensional cloud–resolving mesoscale model based on that of *Mullendore et al.* (2005). The model used f–plane approximation and assumed a latitude of 37°N. The mesoscale processes being investigated occurred on a radiative time scale less than 12 hours, therefore radiation was neglected in the simulation to save computational expense. The cloud microphysics included in this model were a single–moment scheme based on *Lin et al.* (1983). The liquid and ice were assumed to have a spherical shape and were broken into five distributions. There was an open vertical boundary and open lateral boundaries, making the only physical boundary the ground. The domain was 750 km by 475 km by 19.85 km, had a horizontal resolution of 1 km, a vertical resolution of 100 m, and a time step

of 1 second (see figure 2). To avoid spurious reflection of waves at the boundaries, the analysis grid cut off 15 km from the horizontal boundary and 1.85 km from the model top.

An important part of this study was determining the impact of one convective cell. To reduce the available potential energy, an area of dry boundary layer air was added to the domain, which suppressed the continuous growth of new convection. A 30 km transition zone, beginning at 160 km, was placed between the moist boundary layer air (to the left, or west) and the dry boundary layer air (to the right, or east), shown in figure 2. In the transition zone, water vapor decreased linearly with x (figure 3D provides a profile view of the water vapor mixing ratio in the moist section of the domain). It should be noted that the inclusion of the dry boundary layer air suppressed the growth of several additional cells, but additional convection was present in the domain throughout the simulation.

A single sounding was used to initialize the model. The potential temperature, $\overline{\theta}$, was given by

$$
\overline{\theta(z)} = \begin{cases} \theta_0 + (\theta_{tr} - \theta_0)\left(\frac{z}{z_{tr}}\right)^{\frac{5}{4}} & \text{for } z \leq z_{tr} \\ \theta_{tr} exp[\frac{g}{c_p T_{tr}}(z - z_{tr})] & \text{for } z > z_{tr} \end{cases} \tag{3.1}
$$

where θ_0 is the potential temperature at the surface, θ_{tr} is the potential temperature at the tropopause, z_{tr} is the primary tropopause height, c_p is the specific heat of dry air, and T_{tr} is the temperature at the tropopause (*Weisman and Klemp*, 1982). The sounding was isothermal above the tropopause (figure 3A). Wind shear in the lowest 5 km was modeled off of the idealized supercell case in *Mullendore et al.* (2005) (figure 3E and 3F). The water vapor profile was also given by *Weisman and Klemp* (1982), but was adjusted such that water vapor decreased to 0 g kg^{-1} at
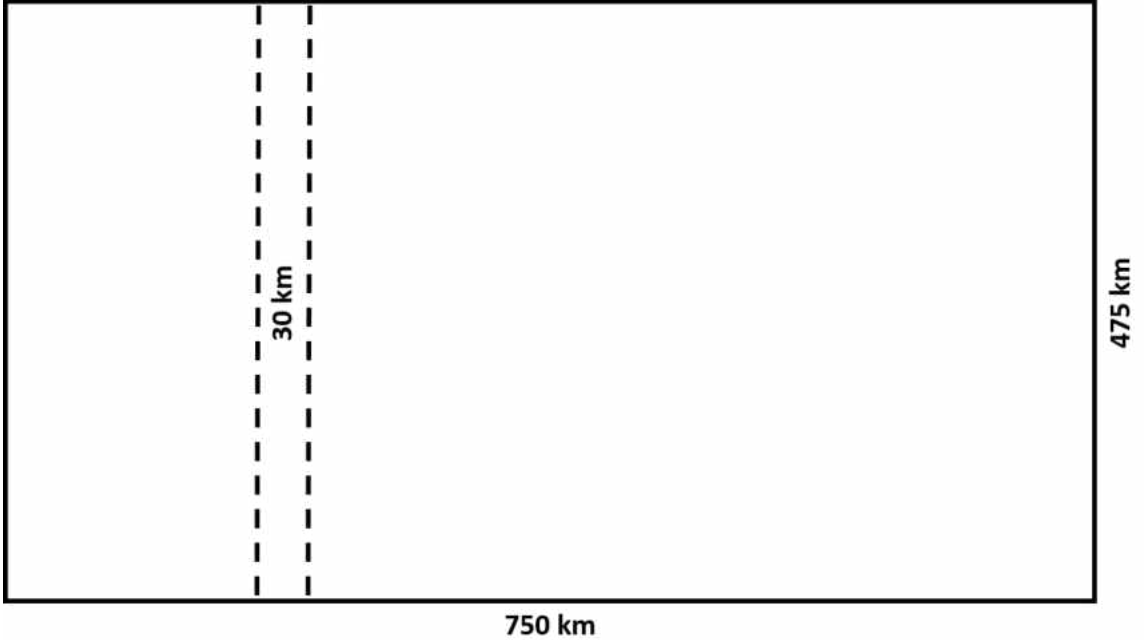
Figure 2: The domain used for the storm simulation. A moist boundary layer is located to the left (west) of the dashed lines, and a dry boundary layer is located to the right (east) of the dashed lines.

approximately 9.85 km to the model top. The original cell was initialized in the moist section of the domain using an instantaneous thermal bubble 2 K above the environmental temperature. This method of initialization is not a realistic representation of what is observed in the atmosphere. However, after approximately 15 minutes the storm begins to take on its own characteristics. Since this study is focused on the tropopause placement during active convection and irreversible convective transport, this form of initialization is acceptable. Additionally, the updraft speed is not strong enough to provide significant mass transport at 15 minutes.

3.1.2   Tracer Initialization

A main goal of this study was to quantify the sensitivity of cross-tropopause transport to tropopause definition. To investigate how mass was transported during
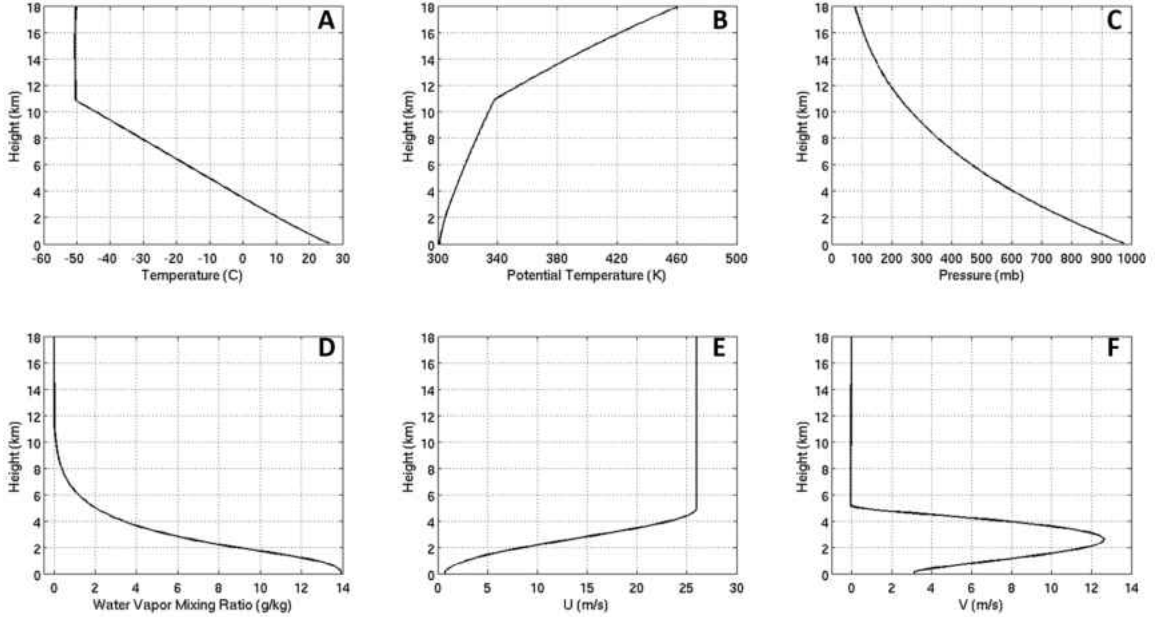
Figure 3: The initial profiles for the input sounding are shown. Plot A shows the initial temperature profile, B shows the potential temperature profile, C shows the pressure profile, D shows the water vapor mixing ratio in the moist section of the domain, E the u-winds, and F shows the v-winds.

the convective event, passive tracers were used. Passive tracers were initially confined within horizontally homogeneous layers, with all areas outside of the layer being zero (figure 4). Three passive tracers were originally confined in layers from 0.1 to 1.45 km, 1.65 to 5.15 km, and 10.85 km to 19.85 km (the model top). The lowest tracer, TR3 in figure 4, represents a boundary layer tracer which is the focus of this study. The mid–tropospheric tracer, TR2, was not evaluated in this study. The stratospheric tracer, TR1, was used as a tropopause definition. The goal of this study was to determine the sensitivity of irreversible boundary layer tracer transport to tropopause definition, therefore TR1 was only evaluated as a tropopause definition and was not evaluated for downward transport into the troposphere.

19
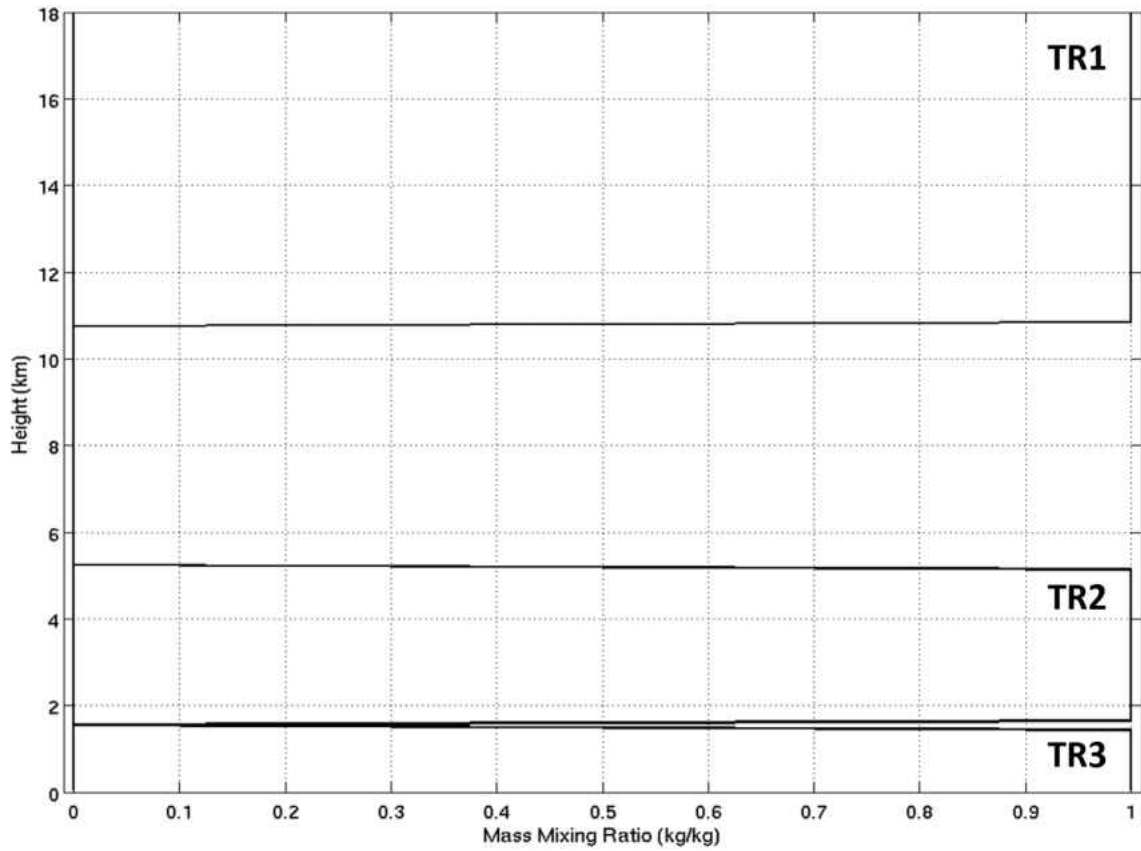
Figure 4: Vertical profile showing the initial mixing ratio for the three passive tracers. TR3 serves as a proxy for a boundary layer tracer and TR1 serves as a proxy for stratospheric tracer.

3.1.3 Storm Evolution and Dissipiation

A single updraft cell was present 30 min into the simulation, which reached a height of 11.7 km with a maximum vertical velocity of 36 m s^{-1}. The updraft strength surpassed 50 m s^{-1} at a simulation time of approximately 40 min and remained strong until approximately 1 hour 10 min, shown in figure 6. The eastern edge of the main cell reached the dry boundary layer air region at a simulation time of approximately 45 min, and the storm began to dissipate at that time. All convection had dissipated by approximately 4.5 hours, and the analysis domain returned to a non–convective state in the following hours.

As stated in section 3.1.1, additional convection was present in the domain throughout the simulation even with the inclusion of the dry boundary layer air region. Cells that developed from the bubble initialized at time zero were investigated, referred to here as the analysis storm system. Additional convection that began at approximately 2.75 hours was not investigated. All convection that was not associated with the analysis storm system was masked out. In other words, columns of the domain associated with the additional convection were not included in mass transport calculations. For example, figure 5 depicts all convection present throughout the domain at 3.0 hours. The cells highlighted by the red box are cells that were masked out, or not included in the analysis. In the masking process, the boundary layer tracer transport to the UTLS region was analyzed every 200 m from 9.85 km to 12.85 km to ensure tracer transport from additional convection did not merge with the analysis storm system. At 3.0 hours, tracers transported by the analysis storm complex and the additional convection remained separated. After approximately 6.75 hours, boundary layer tracer lofted by the additional convection began to merge with the analysis cell. Masking out the additional convection became difficult and mass
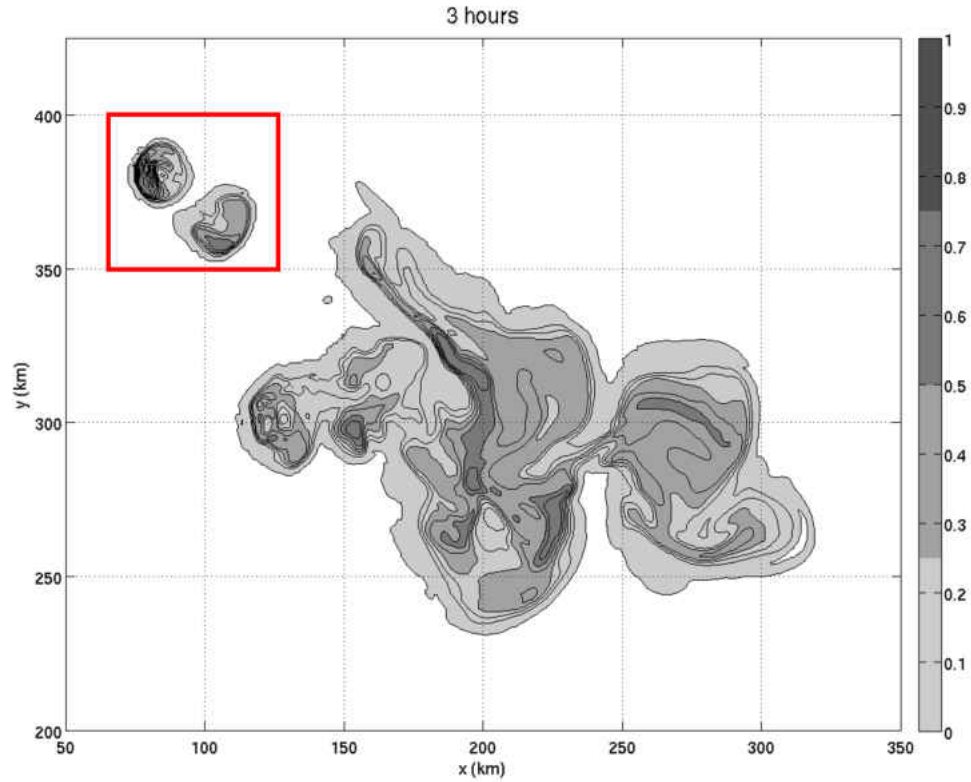
Figure 5: A horizontal cross section depicting the boundary layer tracer at the constant altitude tropopause, 10.85 km, at 3 hours. The grayscale contours represent the boundary layer tracer in kg kg^{-1}. The red box outlines additional convection that was not included in the analysis domain.

in the UTLS region was lost due to the masking. Therefore, results after 6.75 hours should be interpreted with caution.

Two times were chosen for analysis in this study: 1 hour, or the state of active convection, and 10 hours, or the state of post–convection. These times were chosen to evaluate the fluctuations in tropopause height as well as changes in mass transport between the active–convective environment and post–convective environment. Figure 7 depicts the reflectivity at 2 km at 1 hour. The strong updraft is shown here with the maximum reflectivity values exceeding 65 dBZ. Figure 8 depicts the boundary layer tracer present at the constant altitude tropopause at 1 hour, and figure 9 depicts
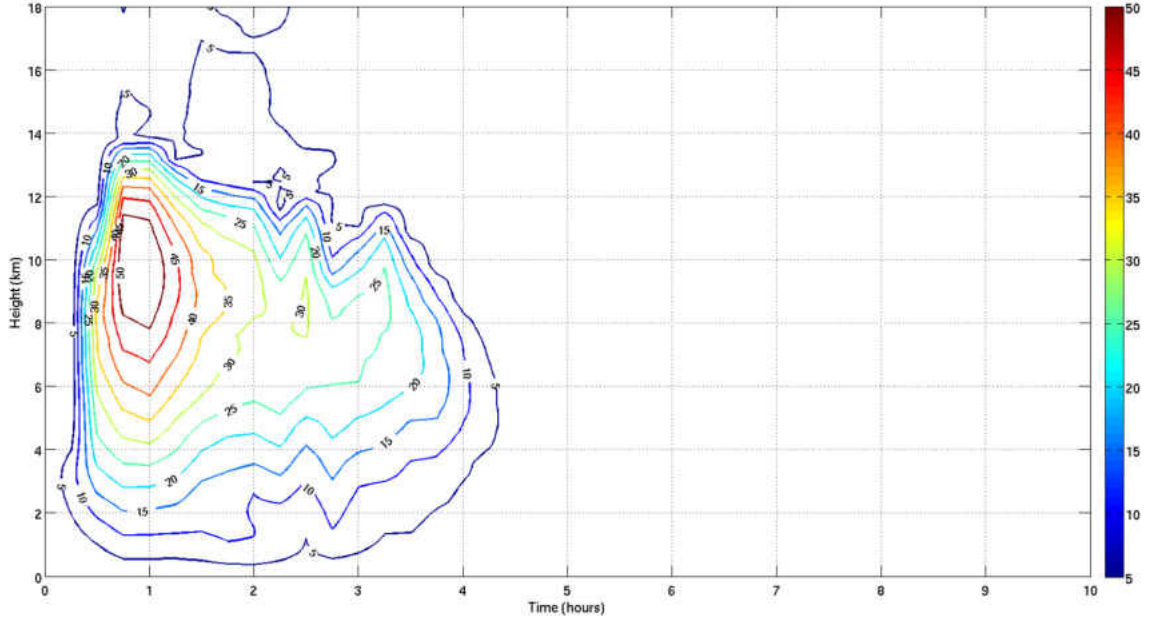
Figure 6: A time–height plot of the maximum vertical velocity at each vertical level throughout the simulation in the analysis domain.

the boundary layer tracer present at the constant altitude tropopause at 10 hours, showing irreversible transport has occurred. To further show the storm evolution, figure 10 shows vertical cross–sections of the boundary layer tracer at three times: 0 hours (the pre–convective environment), 1 hour (the active–convective environment), and 10 hours (the post–convective environment). Again, it is clear when looking at the vertical cross section at 10 hours that irreversible transport has occurred from the boundary layer to the UTLS region.

3.2   Tropopause Calculations

As stated before, the definitions used in this study are those which have been previously published. However, definitions stated in the literature do not necessarily provide the exact method of calculation. To clearly discuss the results of this study, and convey the impact of each definition, the method of calculation for each definition
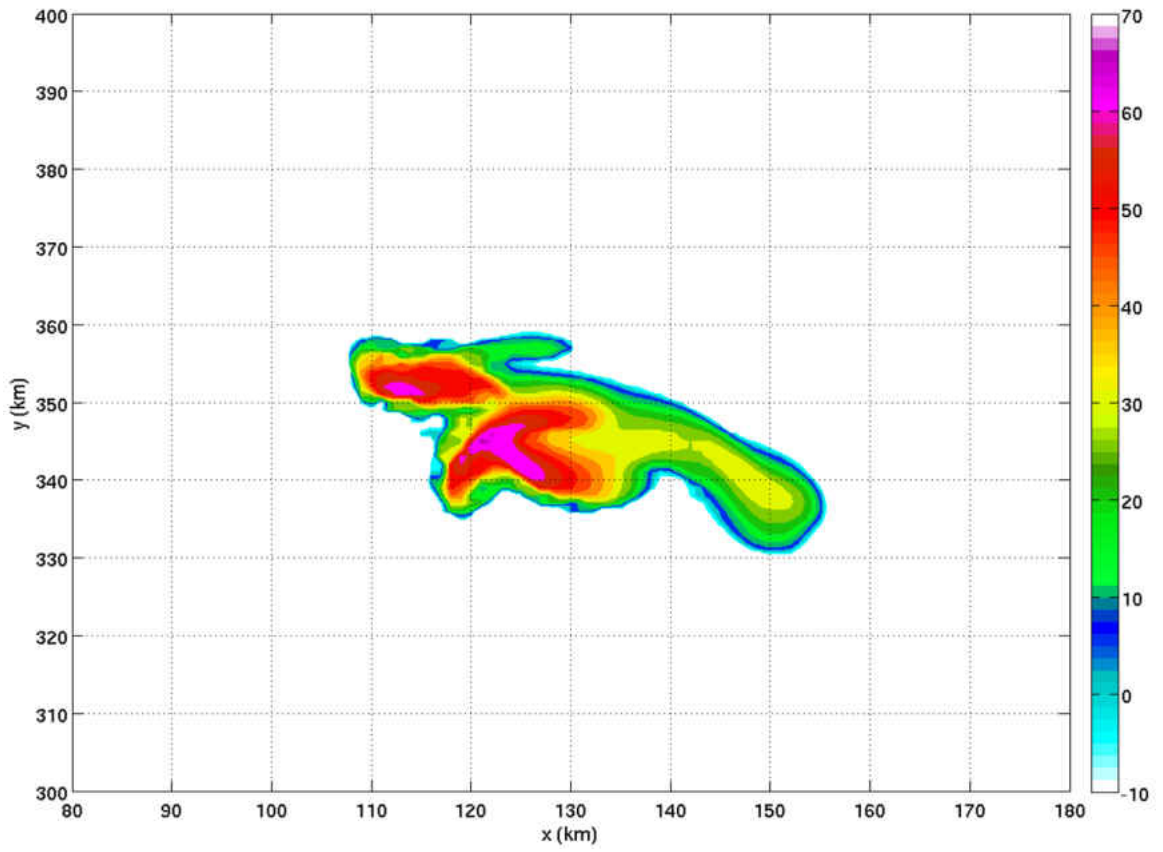
Figure 7: A horizontal cross section depicting the reflectivity at 2 km at 1.0 hours.
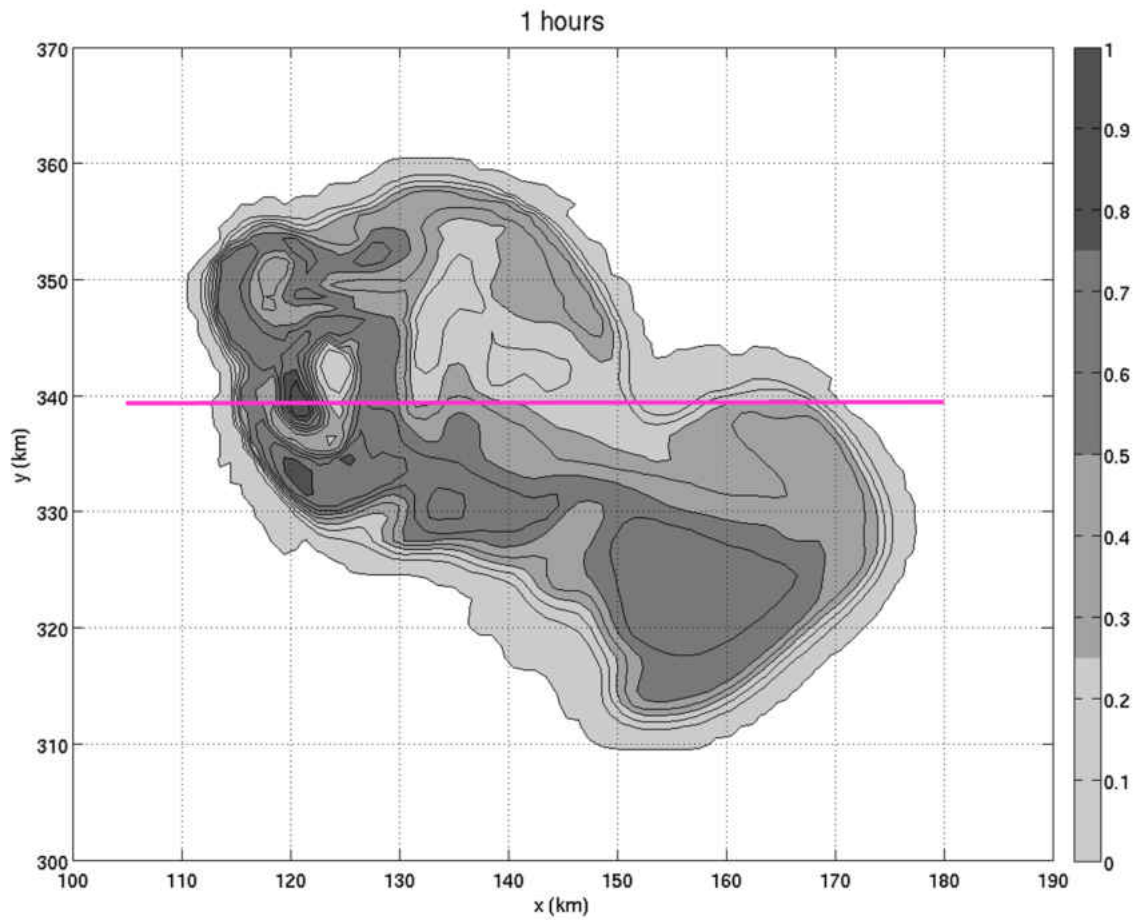
Figure 8: A horizontal cross section depicting the boundary layer tracer at the constant altitude tropopause, 10.85 km, at 1 hour. The grayscale contours represent the boundary layer tracer in kg kg^{-1}. The magenta line represents the location of the vertical cross section shown in figure 10.
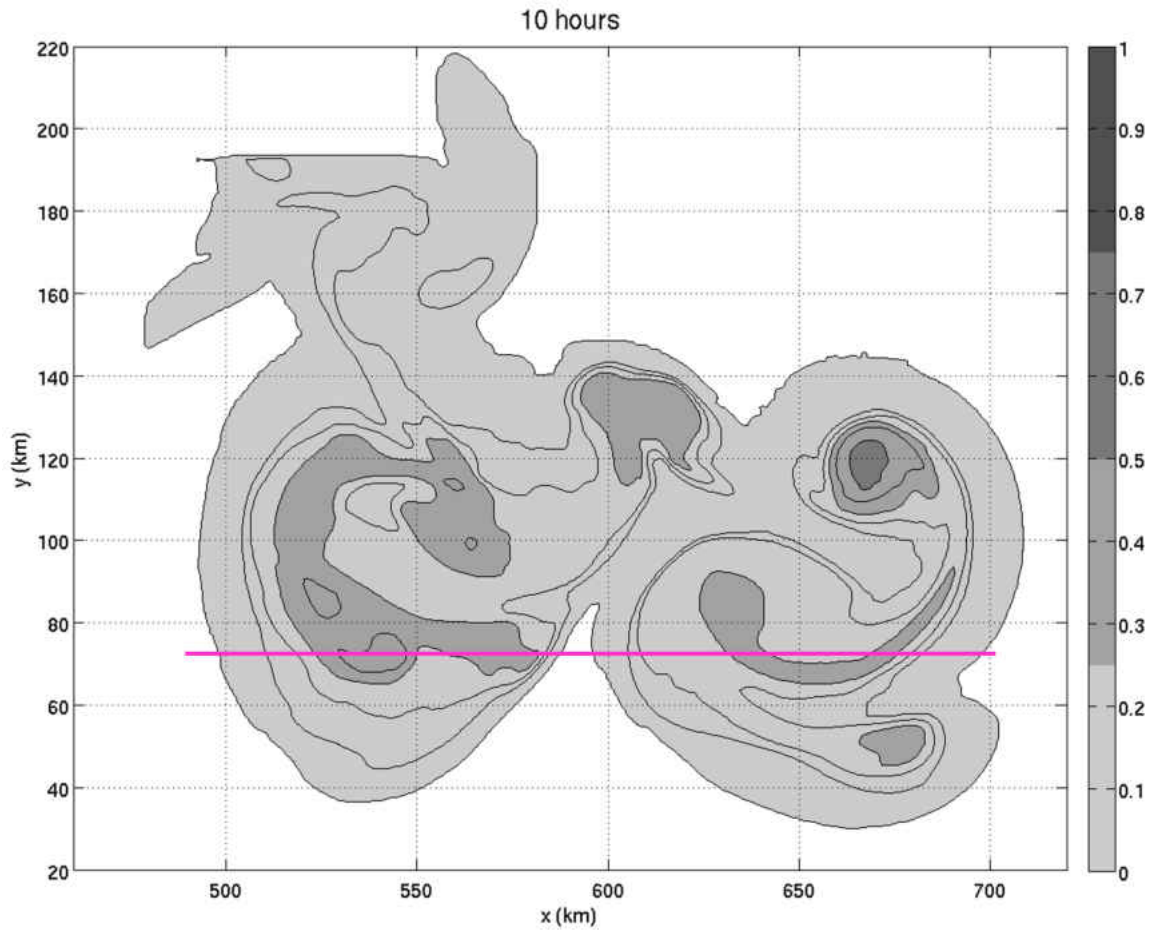
Figure 9: A horizontal cross section depicting the boundary layer tracer at the constant altitude tropopause, 10.85 km, at 10 hours. The grayscale contours represent the boundary layer tracer in kg kg^{-1}. The magenta line represents the location of the vertical cross section shown in figure 10.
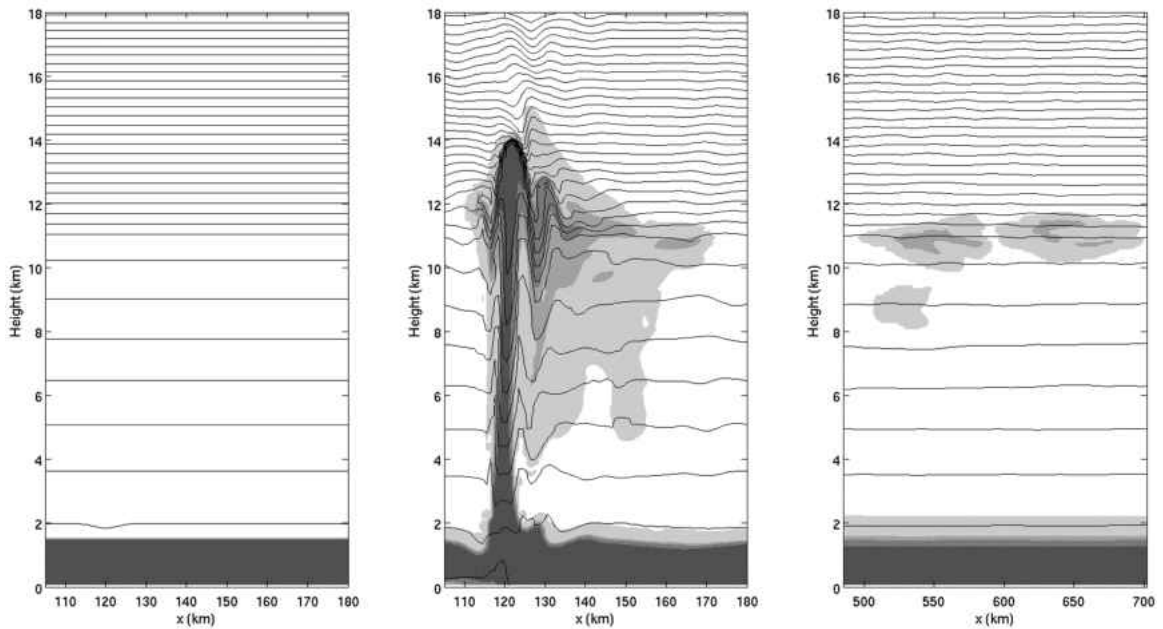
Figure 10: A vertical cross section at the time of initialization (left), through the maximum updraft at 1.0 hours (middle), and through boundary layer tracer remaining in the UTLS region at 10.0 hours (right). Grayscale contours represent boundary layer tracer in kg kg^{-1}, with darker shading representing boundary layer concentrations greater than 0.7 kg kg^{-1}. Thin black lines represent isentropes from 295 K to 500 K with a 5 K contour interval.

is provided below. At all times, the tropopause was restricted to be above 8 km and below 18 km. At the time of initialization, all definitions identified the tropopause at the same altitude as the constant altitude tropopause, 10.85 km. Tropopause calculations used first order forward differencing for all differencing calculations.

3.2.1 WMO

Interpretation I

First, the temperature lapse rate, $\Gamma = -\frac{\Delta T}{\Delta z}$, was calculated for every vertical level in the selected profile.

Then the 2 km vertical average lapse rate was calculated. This was done by summing up the local lapse rate at every point 2 km above the evaluation point (the evaluation point and the 19 points above the evaluation point), then was divided by the number of points (in this case 20 points).

If the local lapse rate and the 2 km vertical average lapse rate above the point met were less than 2 K km^{-1}, that point was defined as the tropopause. If the criteria were not met, the next point in the vertical profile would be evaluated.

Interpretation II

This interpretation was modeled after the method used in *Homeyer et al.* (2014).

First, the temperature lapse rate was calculated for every vertical level in the selected profile. The first altitude that had an local lapse rate less than 2 K km^{-1} was selected as the possible tropopause.

Using the point of the possible tropopause, the average lapse rate between that point and all vertical levels within 2 km was calculated. In other words, using a dz=100 m, 20 averages, using the single difference between the points, will be calculated. If all average lapse rates between the possible tropopause and 2 km above

that point are less than 2 K km^{-1}, that point is identified as the tropopause. If the criteria were not met, the process began again starting with the next occurrence of the local lapse rate which met the WMO criteria.

3.2.2 PV

First, using Ertel's Potential Vorticity Theorem,

$$PV = \frac{1}{\rho}\left[\left(\frac{\partial v}{\partial x} - \frac{\partial u}{\partial y}\right) + f\right] * \frac{\partial \theta}{\partial z}, \tag{3.2}$$

where ρ is density, v and u are horizontal velocity, f is friction, and θ is potential temperature, the potential vorticity was calculated throughout the analysis domain. In the calculations, it was assumed $\frac{\partial v}{\partial x} = \frac{\Delta v}{\Delta x}$, $\frac{\partial u}{\partial v} = \frac{\Delta u}{\Delta y}$, and $\frac{\partial \theta}{\partial z} = \frac{\Delta \theta}{\Delta z}$. Then, using the conversion of $1PVU = 10^{-6}Km^2kg^{-1}s^{-1}$, PV was converted to PVU.

At the time of initialization, a PVU threshold was chosen to represent the constant altitude tropopause. In this study, the PVU threshold found to best fit the constant altitude tropopause was 2.89 PVU. When a vertical profile was evaluated, the first altitude at which the PVU threshold was exceeded was identified as the tropopause height.

3.2.3 Stratospheric Tracer

First, a passive tracer was initialized in the stratosphere only (10.85 km to the model top). In this study, a threshold of 0.5 kg kg^{-1} was chosen to represent the tropopause. In other words, an altitude must contain at least 50% stratospheric air to be considered in the stratosphere. When evaluating a vertical column, the first altitude at which the stratospheric tracer concentration was equivalent to or greater than the designated threshold was identified as the tropopause.

3.2.4 Static Stability

First, the static stability, $\frac{\partial \theta}{\partial z} = \frac{\Delta \theta}{\Delta z}$, was calculated for every vertical level in the selected vertical profile. Similarly to the PV dynamical tropopause definition, a threshold value was chosen at the time of initialization to reflect the constant altitude tropopause, $\frac{d\theta}{dz} = 0.012$ K m^{-1}. The lowest altitude which was equivalent to or exceeded the chosen threshold was identified as the tropopause.

3.2.5 Curvature of the BVF

First, the square of BVF,

$$N^2 = \frac{g}{\theta}\frac{\partial \theta}{\partial z} = \frac{g}{\theta}\frac{\Delta \theta}{\Delta z} \tag{3.3}$$

where g is the gravitational constant, ρ is the density, θ is potential temperature, and z is the altitude, was calculated for each vertical level in the selected profile. Then, the gradient of the BVF, or in this case the difference of the BVF with respect to height (BVF gradient $= \frac{\Delta N}{\Delta z}$) was calculated for every height. The curvature of the BVF, or the difference of the BVF gradient with respect to height,

$$\text{BVF curvature} = \frac{\left(\frac{\Delta N}{\Delta z}\right)_{k+1} - \left(\frac{\Delta N}{\Delta z}\right)_k}{\Delta z}, \tag{3.4}$$

was then calculated. Finally, the altitude at which the maximum curvature was located was identified as the tropopause.

3.2.6 Alternate Tropopause Calculations

As was mentioned in section 2.4.3 and 2.4.6, not all definitions used in this study were intended for use on such small scales. The model used in this study had

a vertical resolution of 100 m, allowing it to resolve smaller dynamical processes. Models used in large–scale studies generally have coarser resolutions. To effectively smooth out the convection and analyze it at a coarser resolution without performing a new model run, a 2 km vertical average was used, modeled after the WMO thermal tropopause definition. Definitions evaluated using this 2 km vertical average included PV, static stability, and curvature of the BVF.

CHAPTER 4

IDEALIZED INVESTIGATION OF MASS TRANSPORT

Six tropopause definitions, previously discussed, were used to analyze irreversible convective mass transport using the UWCOMMAS model described in section 3.1.1. In this chapter, the evolution of the tropopause is evaluated. The sensitivity of troposphere–to–stratosphere transport to each definition, defined through sections 2.4 and 3.2, is tested. Additionally, the alternate calculations described in section 3.2.6.

4.1   Tropopause Evolution

The location of the tropopause, the lower bound of the stratosphere, impacts the quantity of mass located in the lower stratosphere. During a convective event, the tropopause can be displaced several kilometers, making it difficult to accurately determine the tropopause height due to the dynamical processes happening in the storm. After convection has dissipated, areas of the domain which were impacted by the event often have an increased tropopause height. The dynamical impacts of the storm on tropopause placement make it important for definitions to properly track the tropopause placement throughout storm evolution and displacement when tracking the amount of mass above said definition. In the pre–convective environment, all tropopause definitions place the tropopause at the same altitude, 10.85 km. During and after the convective event, though, the tropopause definitions were not always in agreement on tropopause placement.

To investigate the tropopause during active convection, the output at 1.0 hours was evaluated, shown in figure 11 (top). Two definitions, PV and curvature of the BVF, are applicable at synoptic temporal and spatial scales, and generally not chosen for tropopause identification in active convective cases. The PV definition (red line in figure 11) was not appropriate when determining the tropopause location during the convective event. While it was not shown, the tropopause, if unrestricted, reached from the surface to the top of the model in the updraft region. The curvature of the BVF (cyan line in figure 11) also misrepresented the tropopause, but not to the extent of the PV definition. Most misrepresentation of the curvature of the BVF tropopause placement occurred in the anvil regions of the cell. The stratospheric tracer definition (green line in figure 11) placed the tropopause a few hundred meters higher than the remaining definitions. As expected, the definition often mimicked the upper boundary of the 25–50% boundary layer tracer. Recall that an altitude must contain at least 50% stratospheric air to be considered in the stratosphere when using this definition.

Finally, the WMO (blue line in figure 11) and static stability (magenta line in figure 11) definitions were in agreement on the tropopause location. The only location of disagreement in tropopause placement was between the updraft and downdraft regions, and small disagreement in tropopause location (100 m difference) at the peak of the updraft. Moving into the anvil region of the storm, the tropopause definitions reflected one another. The similar behavior in tropopause placement of the WMO and static stability definitions was expected as areas with similar static stability have similar temperature lapse rates. In other words, the strong change in lapse rate (both temperature and potential temperature lapse rates) between the troposphere and stratosphere are distinct, with the sharp change occurring at the same altitude in the pre–convective environment.
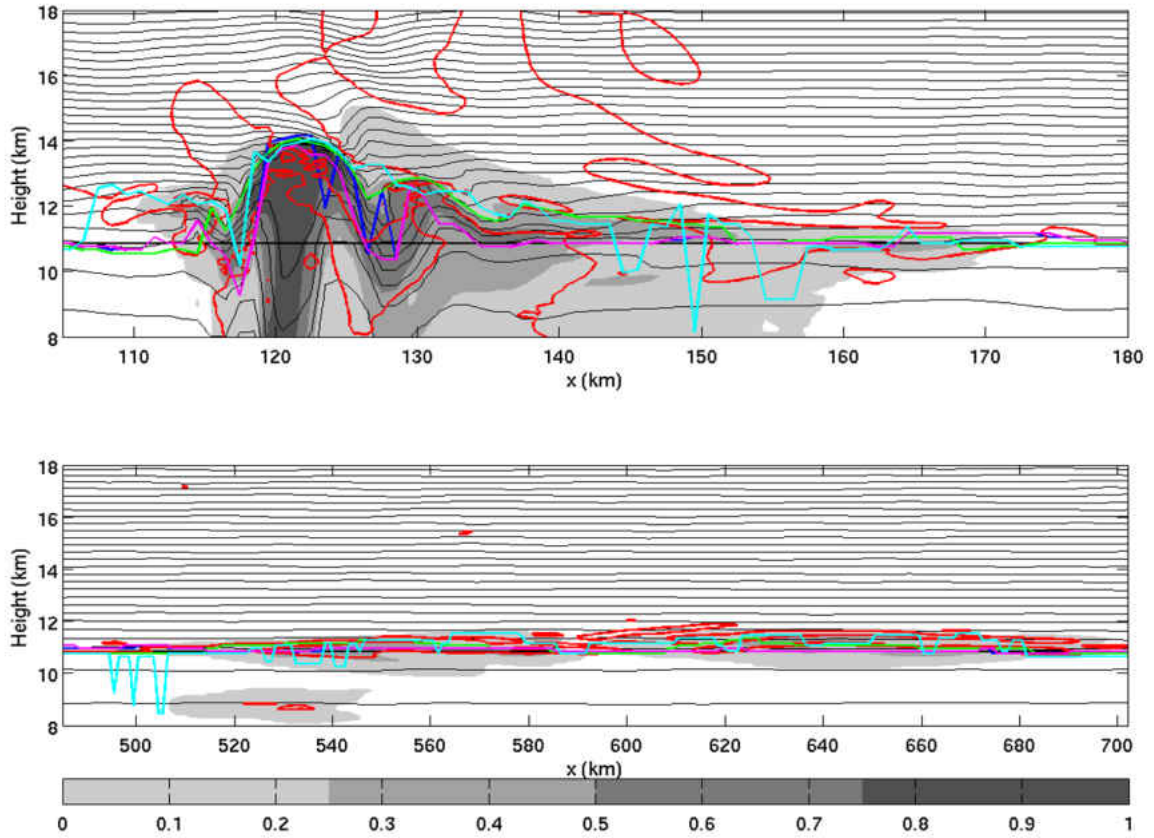
Figure 11: A vertical cross section at 1.0 hours (top) and 10.0 hours (bottom). Grayscale contours represent boundary layer tracer in kg kg^{-1}, with darker shading representing boundary layer concentrations greater than 0.75 kg kg^{-1}. The minimum boundary layer concentration depicted is 0.001 kg kg^{-1}. Thin black lines represent isentropes with a 5 K contour interval. The thick black line represents the constant altitude tropopause, blue represents the WMO thermal tropopause, red represents the PV tropopause, green represents the stratospheric tracer tropopause, magenta represents the static stability tropopause, and cyan represents the Curvature of the BVF tropopause.

A time of 10.0 hours was evaluated to determine tropopause height in the post–convective environment, again shown in figure 11 (bottom). At this time, the PV tropopause was placed near 10.85 km, but it continued to place contours both above and below the 10.85 km altitude. These PV anomalies persisted after all convection had dissipated because no additional synoptic–scale shearing or mixing events took place in the model. These event include mixing at cloud boundaries, mixing around the subtropical jet, and clear air turbulence. The normal deformation of fields such as PV mix to smaller and smaller scales over time through these events. The curvature of the BVF tropopause continued to be misrepresented. However, it was often only misrepresented by 100-1000 meters rather than several kilometers like during the active convective state. The misrepresentations were evident at locations where boundary layer tracer remained in the UTLS region. The definition was most often placed a few hundred meters higher than other definitions, which caused the definition to underestimate the amount of mass transported, discussed in section 4.2. The stratospheric tracer tropopause was often placed approximately 100 m below the remaining definitions where boundary layer tracer was not present in the UTLS region, due to subsidence. It was often placed 100–500 m higher than the remaining definitions in areas with boundary layer tracer present, due to the threshold constraint of 50% stratospheric air discussed above. Finally, the WMO and static stability definitions were nearly always in agreement in tropopause location. There were a few instances where the tropopause was placed with a 100 m difference, but overall the tropopause placement was very similar.

4.2   Irreversible Transport

The main goal of this study was to determine the sensitivity of irreversible cross–tropopause transport to tropopause definition. To do this, the amount of mass
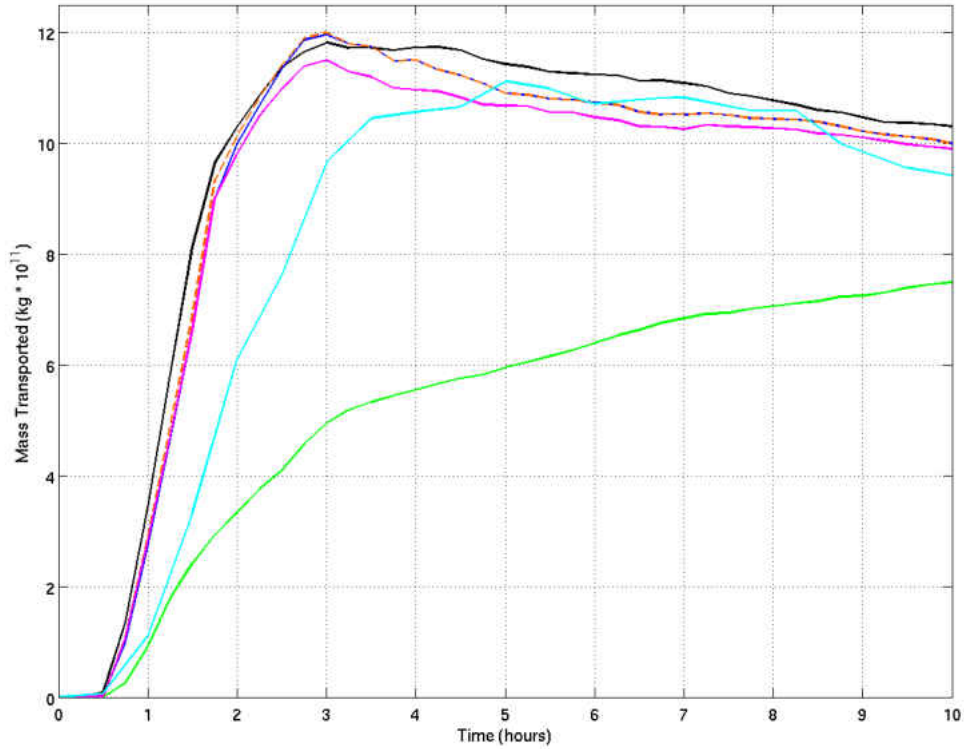
Figure 12: Mass transported above each tropopause definition is shown. Definitions shown are: constant altitude (black), WMO interpretation I (blue), WMO interpretation II (orange), stratospheric tracer (green), static stability (magenta), and curvature of BVF (cyan). The PV definition was not considered in this calculation because of its misrepresentation of the tropopause location both during and after convective events.

that was transported above each tropopause definition throughout the storm simulation was analyzed, with a focus on 10 hours. Figure 12 shows the total mass transported above each definition throughout the 10 hour period and will be discussed in more detail in the following subsections.

4.2.1   Irreversible Transport at 6.75 and 10 Hours

To determine the impact of tropopause definition on irreversible transport, times 6.75 hours and 10 hours were evaluated. As discussed in section 3.1.3, all

convection in the analysis domain dissipated around 4.5 hours. After 6.75 hours, possible contamination occurred from nearby convection that was not included in the analysis of the original cell. The contamination can influence the amount of mass transported above each definition, causing mass to be lost in the later hours of the simulation rather than leveling off (shown through hours 7–10 in figure 12). In these calculations, the PV tropopause was not analyzed as it misplaced the tropopause at many locations, causing results much different than the other definitions.

Evaluating 6.75 hours first, using the constant altitude tropopause as a reference, resulted in the largest amount of mass transport, approximately $11.1 * 10^{11}$ kg. Exact quantities of mass transported can be found in table 2. For completeness, table 1 gives mass transport information at 1 hour; however, the 1–hour transport results are not discussed further in this section. As discussed in section 4.1, the WMO and static stability definitions placed the tropopause at similar altitudes both during and after the convective events. Quantitatively, their use as the troposphere–stratosphere boundary results in similar amounts of inferred mass transport. The WMO definition resulted in 5% less mass transport than that found when using the constant altitude tropopause and the static stability definition, 7% less mass transport. The average curvature of the BVF tropopause height at 6.75 hours was approximately 200 m below the WMO definitions, which led to an increase in inferred mass transport when using this definition. Using the curvature of the BVF definition resulted in 2.5% less mass transport than the constant altitude. At this time, using the stratospheric tracer definition resulted in 39% less mass transport than the constant altitude definition.

Now evaluating 10 hours, using the constant altitude tropopause resulted again in the largest amount of mass transport, $10.3 * 10^{11}$ kg. Exact quantities of mass transport can be found in table 3. Again, shown in figure 12, the WMO and static stability definitions appeared to infer similar amounts of mass transport. The WMO

Table 1: Table showing the analysis grid average tropopause height at 1 hour, total mass transported above the tropopause, and absolute and relative difference of mass transport with respect to the constant altitude tropopause definition. The constant altitude tropopause definition calculated $3.4 * 10^{11}$ kg of mass above the tropopause at 1 hour.

1 hour				
Definition	Average Tropopause Height (km)	Mass Transport (kg * 10^{11})	Absolute Diff w.r.t CA (kg * 10^{11})	Relative Diff w.r.t. CA (%)
WMO I	10.94	2.7	-0.7	-21
WMO II	10.94	2.9	-0.5	-15
Stratospheric Tracer	10.94	0.9	-2.5	-74
Static Stability	10.95	2.8	-0.6	-18
Curvature of the BVF	10.86	1.1	-2.3	-68

definitions resulted in 3% less mass transport than that found when using the constant altitude tropopause and the static stability definition, 4% less mass transport. Using the curvature of the BVF definition resulted in 9% less mass transport than the constant altitude definition. While the quantity of mass transported was similar to the constant altitude definition, the average tropopause height was increased by 900 m, and varied 100-1000 m in areas where boundary layer tracer remained in the UTLS region. Finally, using the stratospheric tracer definition resulted in 27% less mass transport than the constant altitude definition.

4.2.2 Alternate Tropopause Calculations

Section 4.2.2 discussed alternate calculations of three definitions using a 2 km vertical average, modeled off of the WMO interpretation I. Figure 13 shows the original definitions and the alternate calculations at 1 hour. Using the 2 km vertical average method of WMO interpretation I did not improve the performance of each tropopause definition to make these definitions adequate for convective processes. No

38

Table 2: Table showing the analysis grid average tropopause height at 6.75 hours, total mass transported above the tropopause, and absolute and relative difference of mass transport with respect to the constant altitude tropopause definition. The constant altitude tropopause definition calculated 11.1 * 10^{11} kg of mass above the tropopause at 6.75 hours.

6.75 hours				
Definition	Avgerage Tropopause Height (km)	Mass Transport (kg * 10^{11})	Absolute Diff w.r.t CA (kg * 10^{11})	Relative Diff w.r.t. CA (%)
WMO I	10.88	10.5	-0.6	-5
WMO II	10.88	10.5	-0.6	-5
Stratospheric Tracer	10.86	6.8	-4.3	-39
Static Stability	10.89	10.3	-6.8	-7
Curvature of the BVF	10.69	10.8	-0.3	-2.5

Table 3: Table showing the analysis grid average tropopause height at 10 hours, total mass transported above the tropopause, and absolute and relative difference of mass transport with respect to the constant altitude tropopause definition. The constant altitude tropopause definition calculated 10.3 * 10^{11} kg of mass above the tropopause at 10 hours.

10 hours				
Definition	Avgerage Tropopause Height (km)	Mass Transport (kg * 10^{11})	Absolute Diff w.r.t CA (kg * 10^{11})	Relative Diff w.r.t. CA (%)
WMO I	10.89	10.0	-0.3	-3
WMO II	10.90	10.0	-0.3	-3
Stratospheric Tracer	10.82	7.5	-2.8	-27
Static Stability	10.89	9.9	-0.4	-4
Curvature of the BVF	11.75	9.4	-0.9	-9

improvement was seen in the PV definition as contours continued to to reach from 8–18 km. The alternate calculation for the curvature of the BVF continued to show spikes in the tropopause location. The peaks were most often below that of the original calculation. The alternate calculation provided several locations where the definition was estimated to be at a lower altitude. Overall, the alternate calculation of the curvature of the BVF resulted in an underestimate of tropopause altitude compared to the original curvature of the BVF calculation. Since the definitions continued to misidentify the tropopause, the alternate calculations were not considered for mass transport calculations. Although already a good performer, static stability was also tested with this 2 km vertical averaging method; no significant improvement was observed.

4.2.3   Discussion of Sensitivities

In addition to mass transport sensitivity to tropopause definition, there may be important sensitivities to methods used to determine individual tropopause types. Since different definitions may be interpreted in various ways, such as the WMO interpretations presented earlier, it is important to investigate how calculation choices may influence tropopause placement. When definitions are sensitive to these calculation choices, it is important to clearly communicate them in the literature.

4.2.3.1   The Impact of Thresholds

Several definitions in this study used threshold values. However, having to subjectively choose threshold values allows possible error in mass transport calculations. For example, the threshold value chosen for the static stability definition in this study was modeled off of the constant altitude tropopause at the time of initialization. A value of 0.012 K m^{-1} was found to be most representative of the tropopause,
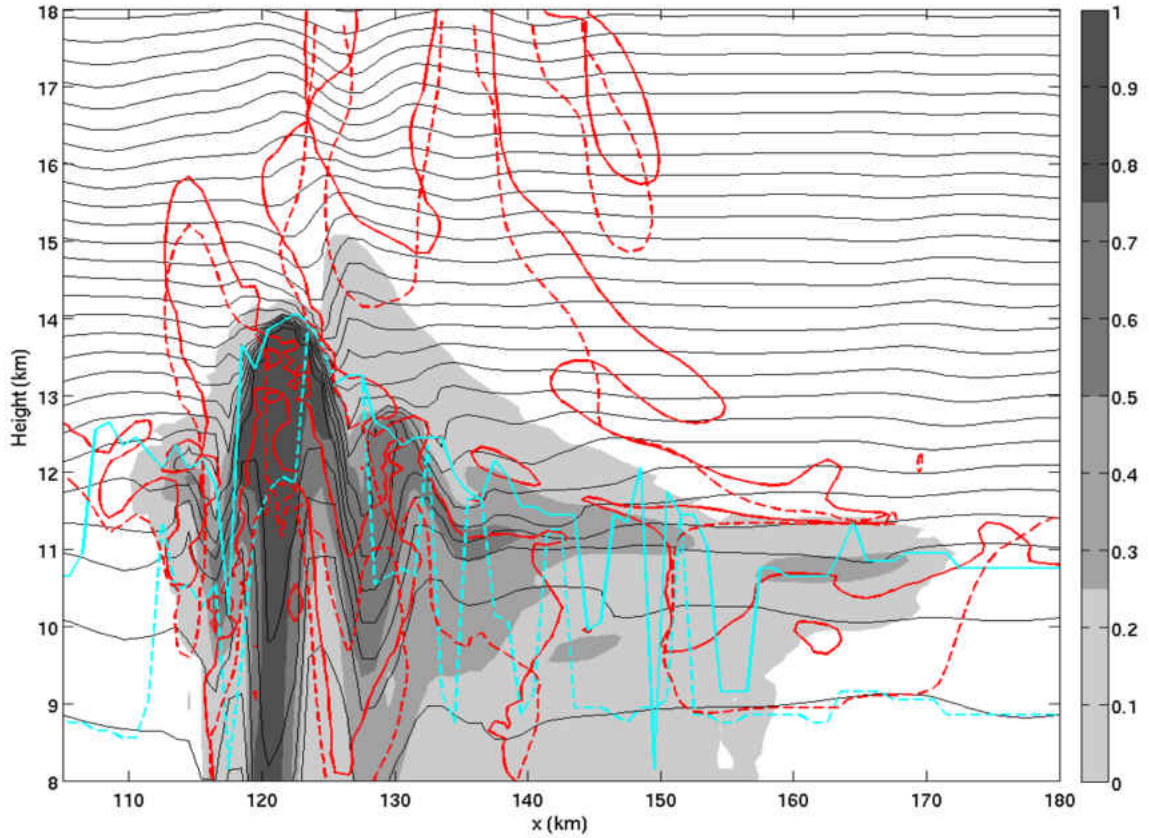
Figure 13: A vertical cross section through the maximum updraft at 1.0 hours. This figure focuses on the UTLS region, 8–18 km. Solid lines represent the original calculation, and dashed lines represent the alternate 2 km vertical average calculation. Red again represents the PV tropopause and cyan represents the curvature of the BVF tropopause. Grayscale contours represent boundary layer tracer in kg kg^{-1}. The minimum boundary layer concentration depicted is 0.001 kg kg^{-1}. Thin black lines represent isentropes from 295 K to 500 K, with a 5 K interval.

41

compared to the value of 0.00935 K m^{-1} used in *Mullendore et al.* (2005). If the value from *Mullendore et al.* (2005) had been used, the total mass transported would have increased by 11%. At this time, using the static stability definition requires the user to have knowledge of the pre–convective environment which may be difficult in real–world case studies. Since mass transport is sensitive to the threshold used, it is very important that threshold values are representative of the tropopause height in the unperturbed atmosphere.

A second example of threshold dependence in this study was the stratospheric tracer definition. A threshold of 0.5 kg kg^{-1} was chosen, meaning at least 50% of the air had to be stratospheric for an altitude to be considered in the stratosphere. However, to the author's knowledge, there is currently no standard for passive tracer threshold. To test threshold dependence here, the threshold was increased and decreased by 10% to evaluate the impact on tracer transport. Decreasing the threshold by 10% resulted in a 12% increase in mass transport, compared to the 0.5 kg kg^{-1} threshold. Increasing the threshold by 10% resulted in a 16% decrease in mass transport. These simple fluctuations in threshold values show the importance of clearly communicating the thresholds used in the literature. This challenge of choosing a threshold value is present in all studies that use chemical tracers. When comparing the same tracer between studies, it is vital that they use similar thresholds to be able to accurately compare their results.

4.2.3.2   The Impact of Calculation Methods

In this study, first order forward differencing (FOFD) was used for all differencing calculations. As a simple test, the WMO I definition was calculated using FOFD and second order centered differencing (SOCD). At the time of initialization, the SOCD method placed the tropopause 100 m higher than the FOFD method. The

order of differencing is not clearly specified in the WMO definition provided in *WMO* (1957), although it can be argued that forward differencing is implied. This is just one example of calculation choices that are left up to the user. In this example, the impact on tracer transport was approximately 8% less mass transported at 10 hours when using SOCD. More generally, this definition ambiguity shows the importance of more clearly communicating calculation choices in the literature.

A challenge with the PV definition was determining whether a contour of PV should be used or whether the first altitude at which the PV threshold value occurred should be used. PV is typically used as a contour when discussing tropopause height. However, all other definitions in this study used the first occurrence of a threshold value, or a maximum value, to indicate the tropopause height. In definitions such as the WMO thermal tropopause, it was stated that the tropopause was the first altitude at which the average lapse rate met the threshold. Through figure 14, it is clear that both methods do not provide an appropriate placement of the tropopause. Using the contouring approach leads to large amounts of mass being missed in the calculation, whereas using the first occurrence of the threshold value leads to large amounts of mass being included in the calculation, especially areas near the core of the convection. *Gettelman et al.* (2011) notes that PV distributions can often be very complex in the vertical, clearly seen in figure 14. *Miyazaki et al.* (2010) found that vertical mixing will sharpen the vertical PV gradient just below the tropopause which may explain PV contours often occur below other tropopause definitions used in this study in figure 11 (top).

4.2.3.3 WMO Algorithm Interpretation

Section 3.2.1 introduced two calculation interpretations of the WMO thermal tropopause definition. Shown in table 3, both interpretations provide the same
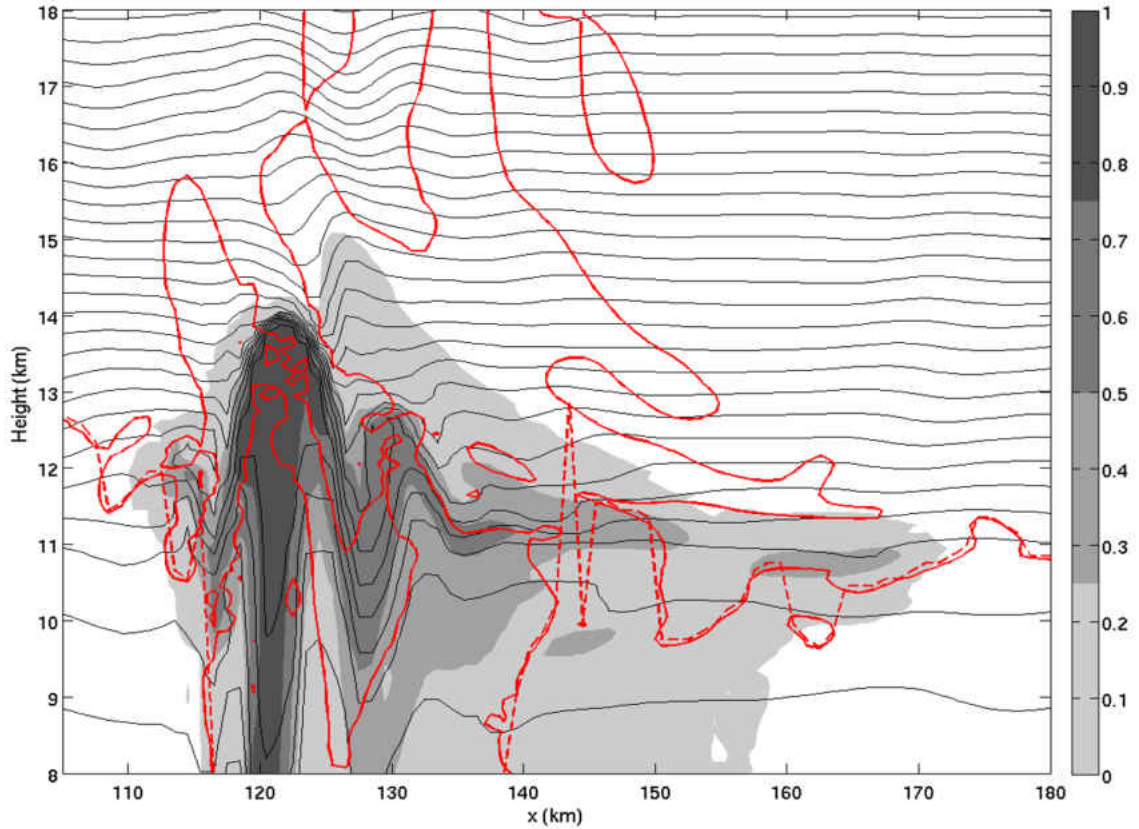
Figure 14: Vertical cross section through the maximum updraft at 1 hour, focusing on 8 km –18 km. Grayscale contours are boundary layer tracer in kg kg^{-1}. The minimum boundary layer concentration depicted is 0.001 kg kg^{-1}. Thin black lines are isentropes from 295 K to 500 K with a contour interval of 5 K, solid red line is the contour of PV, dashed red line is the first altitude at which the PV threshold was met. It should be noted that the tropopause is restricted to be only above 8 km.
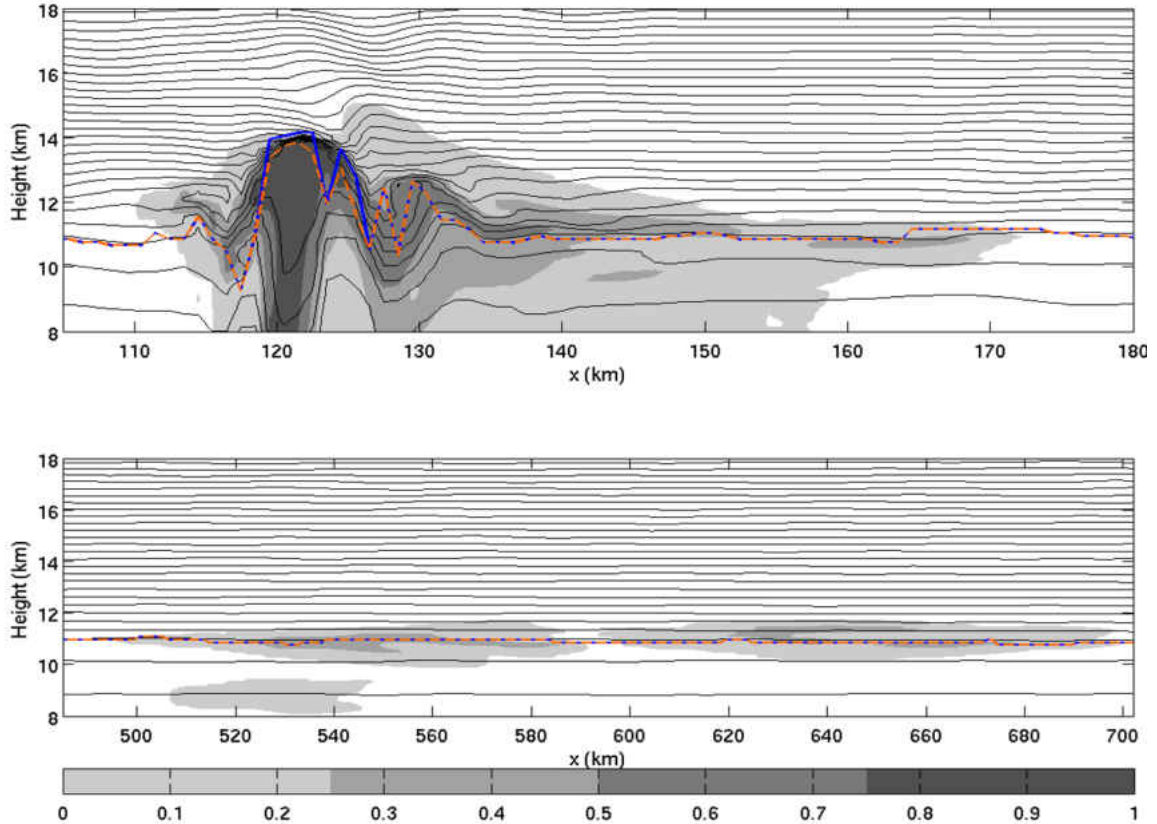
Figure 15: Vertical cross section through the maximum updraft at 1 hour (top) and residual boundary layer tracer at 10 hours (bottom), focusing on 8 km –18 km. Grayscale contours are boundary layer tracer in kg kg^{-1}. The minimum boundary layer concentration depicted is 0.001 kg kg^{-1}. Thin black lines are isentropes with a contour interval of 5 K. The solid blue line represents the WMO Interpretation I tropopause and the dashed black line represents the WMO Interpretation II tropopause, described in section 3.2.1.

amount of mass transported after convection has dissipated. However, during the convective event, the two interpretations provide differing placement of the tropopause, and therefore provides different quantities of mass transported (shown in table 1). Figure 15 depicts a vertical cross section through the updraft core at 1 hour (top) and remaining tracer plume at 10 hour (bottom). In relatively unperturbed areas, the two interpretations provide nearly identical placement of the tropopause, but near the updraft the definitions do not agree on tropopause placement.

Interpretation I uses only the instananeous and 2 km average lapse rate. This definition does not account for temperature fluctuations which may represent tropospheric lapse rates within the 2 km layer. Interpretation II uses the local lapse rate and the average lapse rate between the evaluation point and every point within the 2 km layer. This definition would account for small fluctuations in temperature lapse rate which may represent more tropospheric lapse rates within the 2 km layer. The lapse rates closer to the point being evaluated, such as the lowest 0.5 km in the 2 km layer above the evaluation point, would have a greater influence on determining the tropopause point since those average lapse rates include fewer points. This may be problematic when evaluating structures with an isothermal layer in the stratosphere. Small temperature anomalies would be capable of making the small average lapse rates, such as the average lapse rate 100–200 m above the evaluation point, dismiss the evaluation point as being tropospheric.

4.2.3.4 Model Sensitivities

It should be noted that the horizontal and vertical resolution of the model simulation will impact aspects of the storm such as storm depth, updraft intensity, and mass transport (*Homeyer*, 2015). *Homeyer* (2015) found that transport from the troposphere to stratosphere decreased as Δz decreased, and increased when Δx decreased. He recommended using a $\Delta x = 1$ km and $\Delta z \leq 300$ m when analyzing deep convection, and was used when choosing the resolution for this study.

CHAPTER 5

WRF RESULTS AND DISCUSSION: UNIVERSALITY OF TROPOPAUSE DEFINITIONS IN THE MIDLATITUDES AND TROPICS

Tropopause definitions are considered to be applicable solely in the tropics, in the extratropics, or in both regions. For example, the cold point tropopause is only applicable when discussing a tropical framework, and the PV dynamical tropopause is only applicable when discussing an extratropical framework. Definitions such as the WMO thermal tropopause and static stability tropopause are considered to be applicable in both locations. A simple investigation was performed to test how universal these definitions are between the two regions.

First, a simple thought exercise was performed using two idealized soundings, one from the midlatitudes and one from the tropics. Each sounding was formed using the environmental potential temperature equation provided in *Weisman and Klemp* (1982), shown in section 3.1.1. The surface temperature (25°C), tropopause temperature (-51°C), and tropopause height (10.85 km) were used for the midlatitude case, the storm used in this study based on *Mullendore et al.* (2005). The surface temperature (29°C), tropopause temperature (-82°C), and tropopause height (15.5 km) were used for the tropical case, based off of a WRF simulation performed by *Barber* (2015). The soundings in this example were created such that they have nearly identical stability in the stratosphere, as can be seen in figure 16. The average stratospheric potential temperature lapse rate was 0.018 K m^{-1} in the midlatitude case and was 0.02 K m^{-1} in the tropical case. The average stratospheric temperature
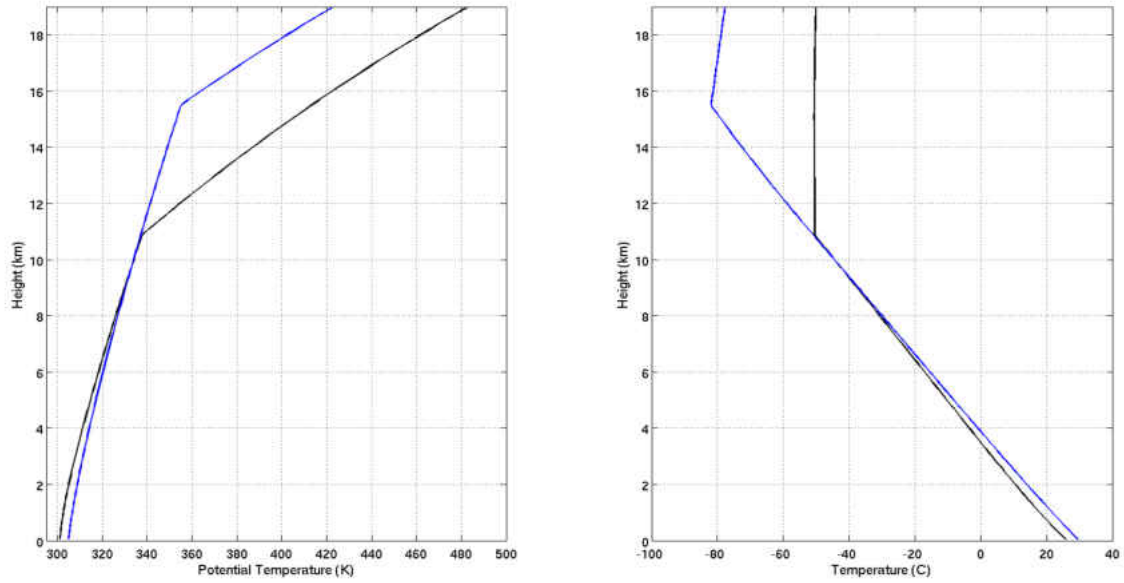
Figure 16: Potential temperature profile (left) and temperature profile (right) for the midlatitudes (black) and tropics (blue).

lapse rate was approximately $0.5°C$ km^{-1} in the midlatitudes case and is $1.2°C$ km^{-1} in the tropical case. Although both stratospheric temperature lapse rates meet the WMO criteria, this simple example shows that profiles with the same stratospheric stability do not necessarily have the same stratospheric temperature lapse rate. Conversely, to make the temperature lapse rate identical for each case, the stability in the stratosphere would then differ more. This shows that lapse rates at specific locations may indicate different levels of stability. Between the midlatitudes and tropics, the tropopause height varies greatly. In this example, the tropopause height differs by approximately 5.3 km. The tropopause height is occurring at different temperatures, clear through figure 16, and different pressure levels.

5.1 Midlatitude and Tropical WRF Simulations

To test the universality of tropopause definitions between the midlatitudes and the tropics, a brief investigation was performed to evaluate tropopause definitions in a more realistic case. Two model simulations, used in *Barber* (2015) and *Barber et al.* (2017), were chosen for this study. One case represented midlatitude convection situated over North Dakota (*Barber et al.*, 2017), the other case represented tropical convection situated near Guam (*Barber*, 2015). The two universal definitions investigated here include the WMO thermal tropopause and the static stability tropopause. Additionally, the PV dynamical tropopause was evaluated in the midlatitude case only, and the cold point tropopause was evaluated in the tropical case only. The cold point tropopause was included because it is a common definition used to study the transport of water vapor from the troposphere to the stratosphere in the tropics, which is to a great extent controlled by the temperature at the cold point tropopause (*Kim and Son*, 2012).

The Weather Research and Forecasting (WRF) model was used to perform the tropical and midlatitude convection studies (*Skamarock et al.*, 2008; *Barber*, 2015; *Barber et al.*, 2017). The microphysics scheme used was WSM-6, cumulus scheme was Kain–Fritsch, longwave radiation scheme was RRTM, shortwave radiation scheme was Dudhia, the land surface scheme was Noah Land Surface Model, the planetary boundary layer scheme used was Mellor–Yamada–Janjić (MYJ), and the surface layer scheme used was the Eta similarity theory for the midlatitude case and MM5 was used for the tropical case. Both simulations used European Reanalysis (ERA)–Interim data. The model top in both simulations was set to 10 hPa, approximately 30 km, with a dampening layer of 10 km in the midlatitude case and 5 km in the tropical case. Both simulations used nested domains.

In this investigation, only tropopause location was evaluated. Unlike the focus of chapter 4, the study of passive tracers was not performed in these simulations. To properly study the transport of tracers, they must be conserved in the simulation. When using nested domains, convection may happen in either domain. While the main focus of analysis is on the inner, finer resolution domain, boundary layer tracers that are transported vertically by convection in the outer domain are able to be transported horizontally into the inner domain (*Bigelbach*, 2013). The convection, and their respective tracers, in the outer domain do not retain the definition seen by convection occurring in the inner domain. This creates possible tracer contamination as these smoothed–out tracer plumes are advected from the outer domain to the inner domain, causing calculations to be less robust.

A 30–hour simulation, beginning at 0000 UTC on 13 July 2005, was performed for the midlatitude case (*Barber et al.*, 2017). The domain was situated over North Dakota, shown in figure 17, where d03 was the analysis grid used in this study. A horizontal resolution of 500 m, with 100 vertical levels, was used for the midlatitudes simulation. Convection on this day was non–severe, with mainly isolated cells that formed along boundaries located in the northern region of ND. Cell development began around 1800 UTC, with 1–km reflectivity values exceeding 40 dBZ between 1800 UTC and 0100 UTC. The simulated convection remained isolated until approximately 2200 UTC, then dissipated around 0100 UTC on 14 July 2005. The maximum simulated echo tops were near 11 km at 2300 UTC, which was chosen as the analysis time in this study.

The initialization time (0000 UTC on 13 July 2005) was used to determine the tropopause height of the unperturbed atmosphere. At this time, convection was not present in the domain. The static stability and PV thresholds were chosen to represent the WMO thermal tropopause, approximately 11 km, shown in figure 18
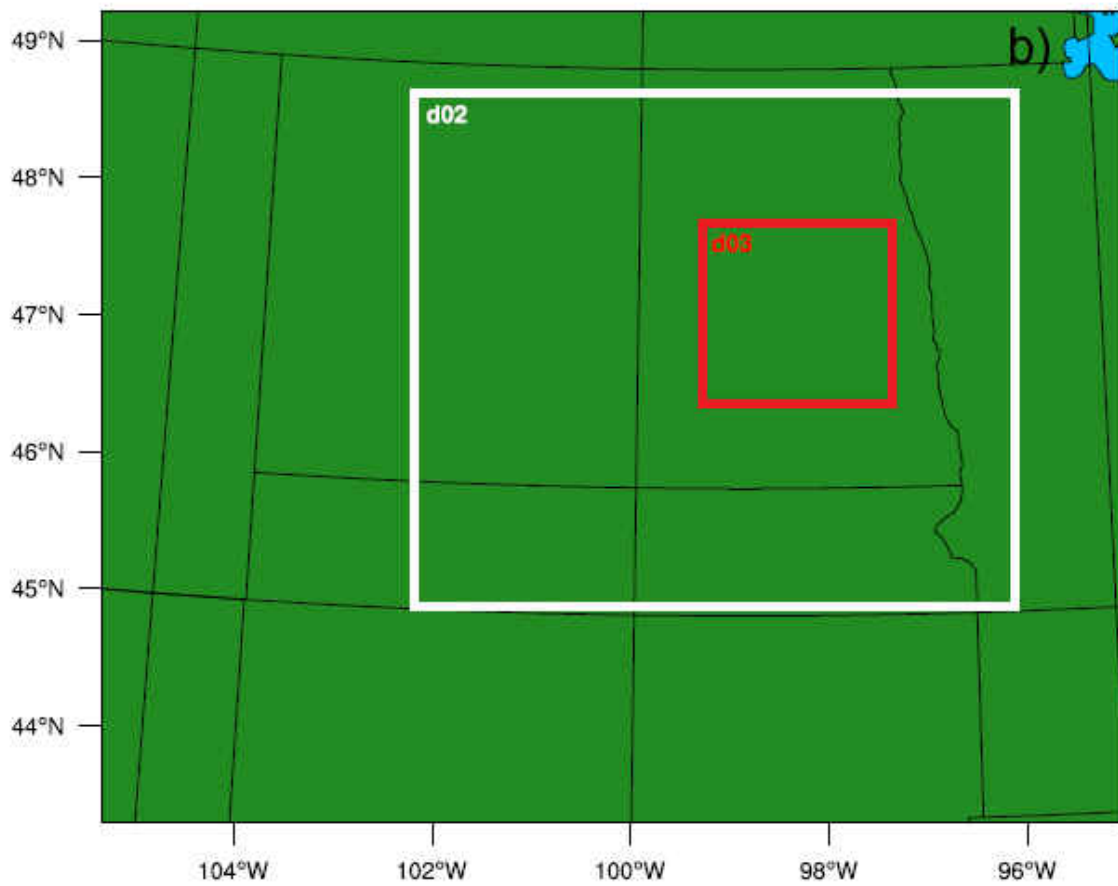
Figure 17: The domain of the midlatitude run situated over North Dakota is shown. Figure is from *Barber* (2015).

(left). The static stability threshold was 0.0115 K m^{-1} and the PV isosurface was 4.03 PVU. While several cells were present in the analysis domain at this time, a cell that remained somewhat isolated from the line of convection was chosen. Figure 19 shows the reflectivity at 1 km. Figure 20 (left) shows a vertical cross section through the updraft of the analysis cell (the magenta line in figure 19). In this cell, the maximum updraft speed was approximately 20 ms^{-1} at 2300 UTC. Unlike the cell investigated in chapter 4, the cell did not extend deeply into the stratosphere at this time. As seen in the previous chapter, the WMO thermal tropopause and static stability tropopause were generally in agreement. Small differences of 100 m were present in a few locations, but overall the definitions provided comparable representations of the tropopause. As expected, the PV dynamical tropopause was generally not in agreement with the other tropopause definitions. However, since the cell being investigated had a weaker updraft, the magnitude of the misidentification by the PV definition was much less than that seen in chapter 4.

A 24–hour simulation, beginning at 0000 UTC on 5 August 2015, was performed for the tropical simulation (*Barber*, 2015). Again, in this study only the inner domain (d03), centered over the Guam (PGUA) radar site, was investigated, shown in figure 21. A horizontal resolution of 1.667 km, with 75 vertical levels, was used. On this day, convection was present in the PGUA radar domain, with echo top heights generally between 6–10 km. Convection in the simulation transitioned from weaker deep convection to more shallow convection. The simulated convection contained mostly small cellular storms, with the addition of larger cells in a linear orientation east of Guam after the twentieth hour which propagated westward.

Similarly to the midlatitude simulation, the initialization time (0000 UTC on 5 August 2015) was used to determine the tropopause height of the unperturbed atmosphere. Again, at that time convection was not present in the domain. For the
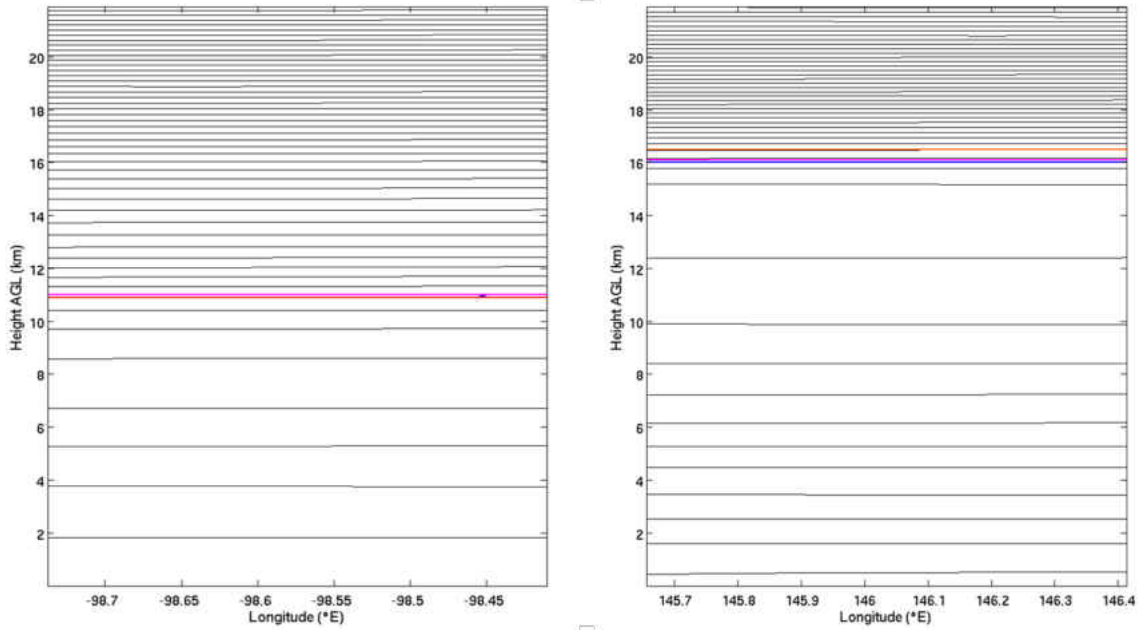
Figure 18: Vertical cross section through the unperturbed atmosphere at 0000 UTC 13 July 2005 for the midlatitude case (left) and at 0000 UTC 5 August 2015 for the tropical case (right). Thin black lines represent isentropes from 295 K to 500 K with a 5 K contour interval. The WMO thermal tropopause is represented in blue, static stability tropopause is represented in magenta, PV dynamical tropopause is represented in red (left only), and cold point tropopause is represented in orange (right only).
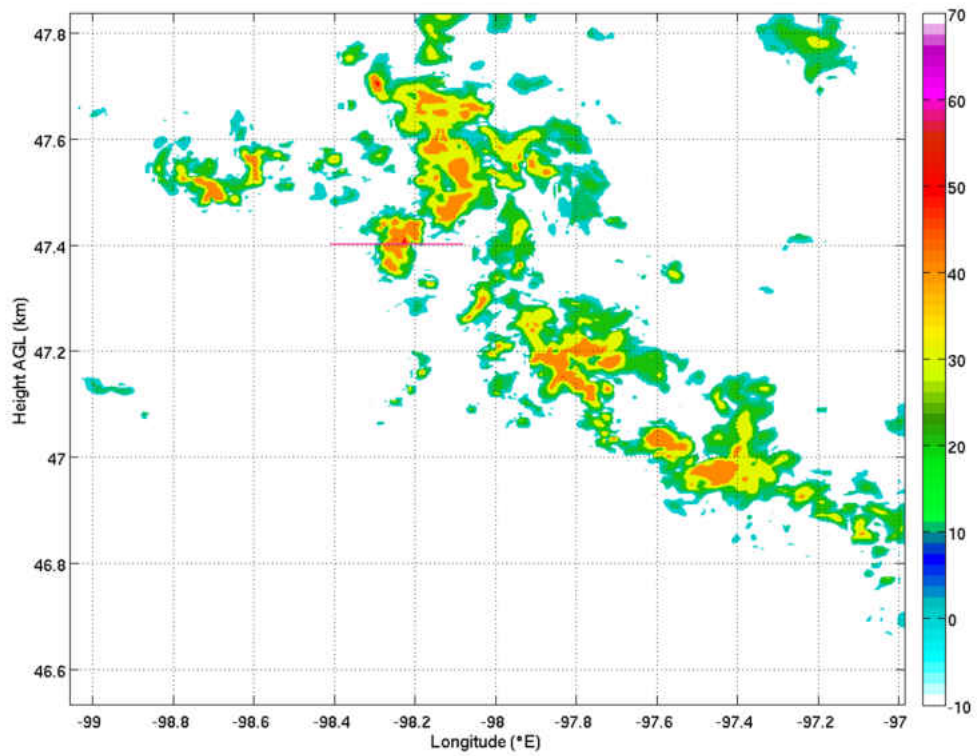
Figure 19: Horizontal cross section at 1 km at 2300 UTC on 13 July 2005 for the midlatitude case. Colored contours are reflectivity in dBZ and the magenta line represents the location of the vertical cross section in figure 20 (left).
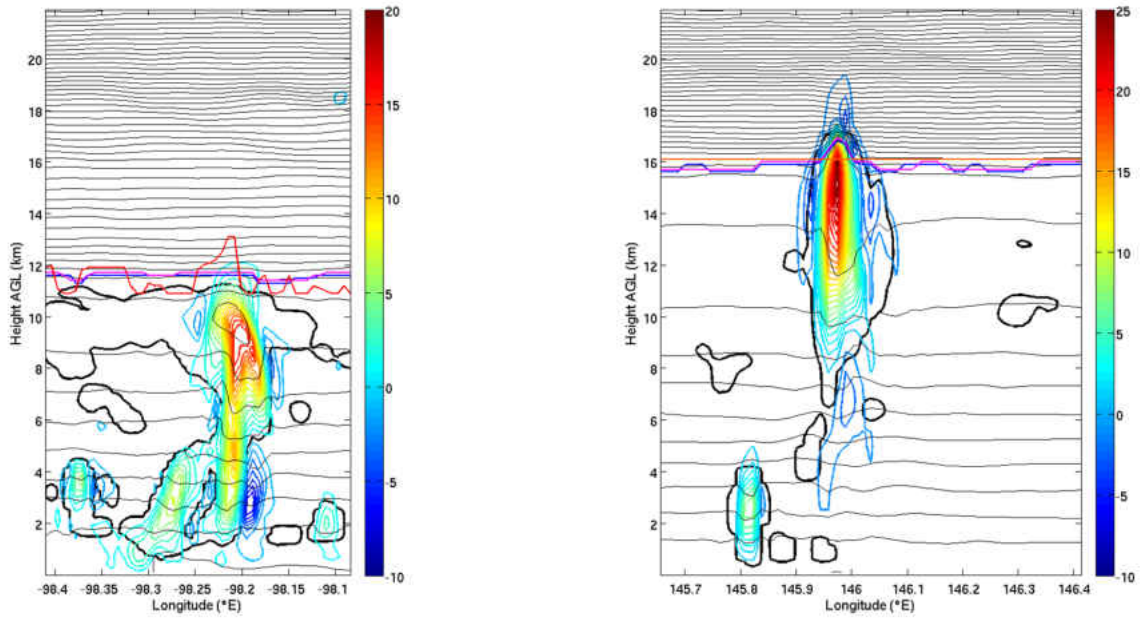
Figure 20: Vertical cross section through the perturbed atmosphere at 2300 UTC 13 July 2005 for the midlatitude case (left) and at 1200 UTC 6 August 2015 for the tropical case (right). Thin black lines represent isentropes from 295 K to 500 K with a 5 K contour interval. Thick black lines represent cloud contour mixing ratio in $1 * 10^{-5}$ g kg^{-1}. Colored contours represent vertical velocity from -10 m s^{-1} to 25 m s^{-1}. The WMO thermal tropopause is represented in blue, static stability tropopause is represented in magenta, PV dynamical tropopause is represented in red (left only), and cold point tropopause is represented in orange (right only).
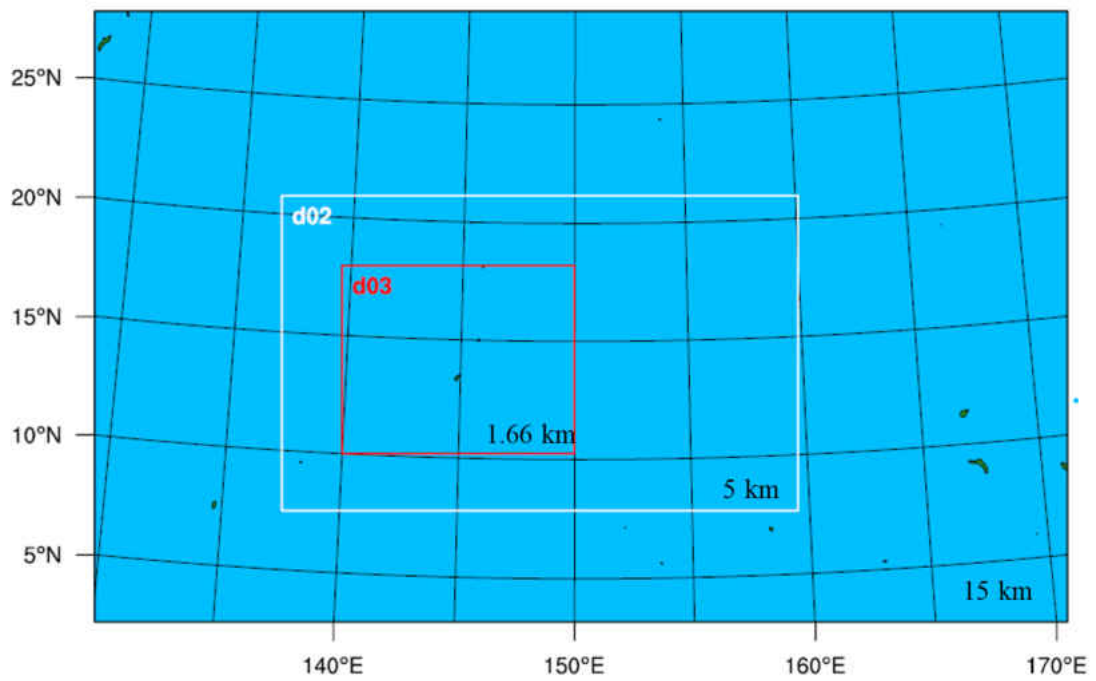
Figure 21: The domain of the tropical run situated over Guam is shown. Figure is from *Barber* (2015).

tropical case, the WMO thermal tropopause, static stability tropopause, and cold point tropopause were evaluated, shown in figure 20 (right). The WMO definition placed the tropopause at approximately 16 km, and the static stability threshold, 0.0135 K m^{-1}, was calculated to reflect the WMO height. The cold point definition placed the tropopause height at a higher altitude, approximately 16.5 km. Once again only one hour, 1200 UTC on 6 August 2015, was evaluated for this case. Figure 22 shows a horizontal cross section of reflectivity at 1 km. At this time, most of the convection remained in isolated cells near the southern edge of the domain. The northern–most cell of this group was chosen to be analyzed to avoid boundary contamination from the southern–most group of convection which had recently advected into the domain. Figure 20 (right) shows a vertical cross section through the convective cell at 1200 UTC (the location is shown by the magenta line in figure 22). The maximum updraft velocity at this time was approximately 25 m s^{-1}, but did not induce large perturbations in the stratosphere at this time. Once again the WMO and static stability definitions generally placed the tropopause at the same altitude. However, the cold point definition showed no change in the tropopause location, despite the stronger updraft present at that location. This finding has been shown in multiple studies, where the cold point tropopause shows little to no change in height in the presence of deep convection (e.g. *Frey et al.* (2015); *Kim and Son* (2012)). For example, *Frey et al.* (2015) found a cold point tropopause change of 0.3 km during a Hector event while ice was injected up to 4 km above the cold point tropopause.

5.1.0.1 Challenges

The model used for the simulation evaluated in chapter 4 was an idealized, three–dimensional cloud–resolving model. This idealized model used a constant vertical grid spacing, whereas the storms evaluated in this section used a WRF setup
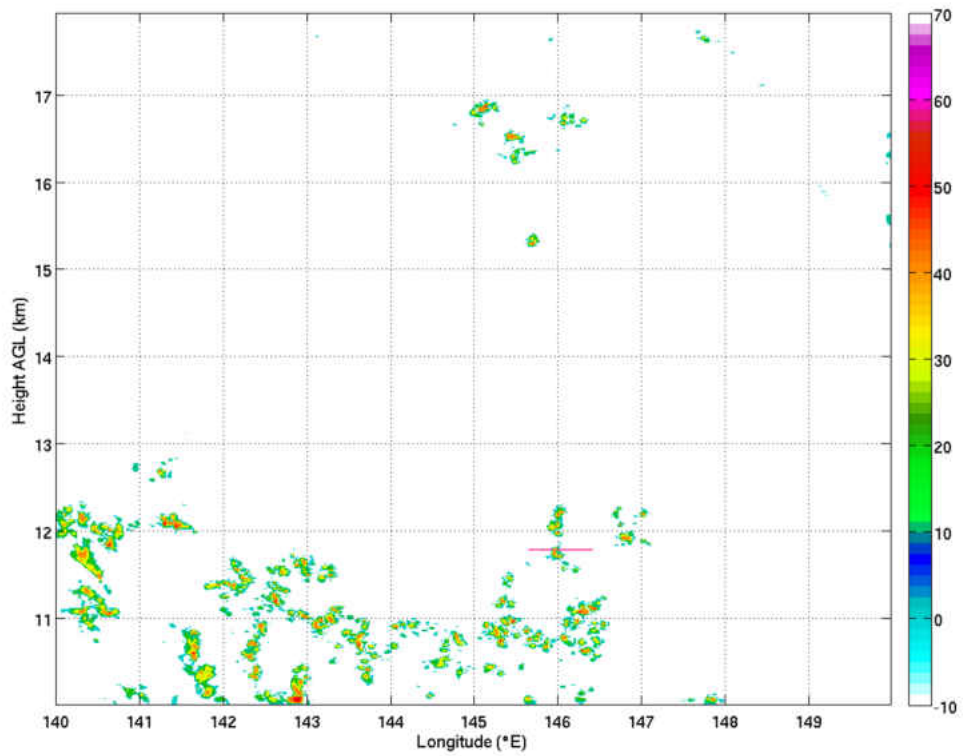
Figure 22: Horizontal cross section at 1 km at 1200 UTC on 6 August 2015 for the tropical case. Colored contours are reflectivity in dBZ and the magenta line represents the location of the vertical cross section in figure 20 (right).

where vertical spacing was not equal at all heights. Changes in vertical grid spacing ranged from approximately 50 m to 500 m. This meant that the data had to be interpolated to a set vertical grid spacing to be calculated using the same methods used in the previous chapter. Additionally, the horizontal resolution of each simulation differed. This should not necessarily impact the tropopause calculations, other than the PV calculation, but as was noted in section 4.2.3.4, the resolution of the model can impact various aspects of the storm.

5.2 Universality of Tropopause Definitions Summary and Conclusions

In this chapter, the regional applicability of the WMO thermal tropopause and static stability tropopause were evaluated. If we once again look at the thought exercise, it was shown that locations with the same lapse rate may not necessarily have the same stability. However, when looking that that particular example, the stratospheric lapse rate in both locations was below the WMO thermal tropopause threshold. Therefore, the definition should have placed the tropopause at the correct height for both regions.

To analyze this further, a small investigation into a midlatitude and tropical convective simulation was performed. As expected based on the findings from chapter 4, both definitions placed the tropopause at approximately the same height in the midlatitude convective case. A similar situation was seen in the tropical case, however, the WMO and static stability definitions had more instances of 100 m differences in tropopause placement in the tropical convective case than the midlatitude convective case. The cold point tropopause was located above the other two definitions both in the unperturbed and perturbed environment. While the WMO thermal tropopause accurately places the tropopause in both idealized and realistic cases, it is worthwhile to note that the WMO definition diagnoses areas with the same temperature lapse

rate, but not areas of the same stability, which has an important role in convective transport.

CHAPTER 6

SUMMARY AND CONCLUSIONS

A three-dimensional cloud-resolving model was used to analyze the sensitivity of cross-tropopause transport to tropopause definition. Convection was suppressed around 1 hour as the main cell entered the dry boundary layer region. All convection dissipated around 4.5 hours. The supercell was simulated out to 10 hours to evaluate irreversible transport of boundary layer air parcels into the lower stratosphere. Possible tracer contamination occurred after 6.75 hours from additional convection in the domain, so results after that time should be interpreted with caution. Air parcels originating in the boundary layer were able to penetrate into the lower stratosphere, and through diabatic processes, were able to become neutrally buoyant at stratospheric altitudes.

Six tropopause definitions were evaluated in this study: constant altitude, WMO, PV, stratospheric tracer, static stability, and curvature of the BVF. Irreversible transport from the boundary layer to the lower stratosphere is dependent on tropopause placement as it dictates the lower bound of the stratosphere, making it vital that the tropopause is placed correctly during and after convective events. Definitions including the PV and curvature of the BVF tropopause were found to misidentify the tropopause in multiple locations, especially near the updraft and downdraft. The PV definition, when not restricted, identified the tropopause from the surface to the model top in the updraft core. Through figure 11, it was clearly shown that PV does not provide a reliable tropopause height during active convection. Additionally,

misidentification of the tropopause continued at 6.75 and 10 hours because the model did not contain additional synoptic–scale stretching and shearing events to mix out the remaining PV anomalies. This definition is not recommended for use in deep convective studies. The curvature of the BVF often misidentified the tropopause height in the anvil region of the storm during active convection. Tropopause placement at 10.0 hours had several locations where the tropopause was estimated to be 100-1000 m higher than the WMO and static stability definitions in areas where boundary layer tracer was present in the UTLS region. This caused the definition to underestimate the amount of mass transported at 10.0 hours. It is recommended that further testing be done on other convective cases using the curvature of the BVF definition. Mass transport values remained similar to definitions considered reliable such as the WMO definition, but tropopause placement was often misrepresented when analyzing vertical cross sections.

The stratospheric tracer definition often placed the tropopause 100-300 m above other definitions (WMO and static stability) during active convection. This definition required that an altitude contain at least 50% stratospheric tracer air to be considered as in the stratosphere. Section 4.2.3.1 discussed the sensitivity of mass transport to the stratospheric tracer threshold, showing that it is sensitive to the chosen threshold. This highlighted the issue that, to the author's knowledge, there are currently no standard threshold values used in the literature. Studies that use the stratospheric tracer threshold method need to use similar threshold values in order to reliably compare the studies. However, regardless of threshold choice, this definition is a poor choice for mass transport studies as it depends solely on a tracer threshold, rather than accounting for thermodynamic processes such as latent heating of the air parcel. For example, a parcel of air originating in the boundary layer may be heated enough while transported through the updraft core to become neutrally buoyant in

the lower stratosphere. This parcel may undergo little mixing with stratospheric air. Even though the parcel is now neutrally buoyant in the stratosphere, if it does not undergo enough mixing with stratospheric air, the parcel would still be considered as tropospheric as it does not contain enough stratospheric tracer. This results in an underestimate of mass transport during and after the convective event because the parcels of undiluted boundary layer air are still considered tropospheric, regardless of their location.

The WMO and static stability tropopause definitions placed the tropopause at similar altitudes both near and away from convection. The definitions, including both interpretations of the WMO calculation, transported similar amounts of mass both during and after the convective event. Both WMO interpretations use generalized criteria, described by *WMO* (1957). The use of these general criteria make the definition applicable in multiple regions because they diagnose altitudes with the same range of temperature lapse rates, not necessarily the same stability. At this time, the static stability method requires the user to identify the proper threshold from the pre–convective environment specific to that convective event. In section 4.2.3.2 it was shown that mass transport is sensitive to the threshold used. This definition has not been widely used in mass transport studies, but further investigation of typical stability profiles and thresholds at the tropopause heights could be used to create general criteria such as that used by the WMO definition. But since the static stability definition currently does not have the general criteria, it is recommended to use the WMO definition. Using the static stability definition could become difficult if the exact pre–convective environment is not known or if several cases are being evaluated, as the threshold will change for each convective event.

An additional small investigation was done to analyze the universality of the WMO and static stability tropopause definitions. A midlatitudes case, situated over

North Dakota, and a tropical case, situated near Guam, were performed by *Barber* (2015). Only the tropopause placement was evaluated in these cases. Results show that the WMO and static stability tropopause definitions provide similar tropopause placement in both locations. However, in the tropical case investigation, the WMO thermal tropopause did not place the tropopause height equal to that of the cold point tropopause. The cold point tropopause was found to remain at the same altitude, regardless of convection, as was found in previous studies (e.g., *Frey et al.* (2015); *Kim and Son* (2012)). Again, it is worthwhile to note that the WMO definition diagnoses area with the same temperature lapse rate, but not necessarily areas of the same stability, which is important to convective transport.

From the findings of this study, it is not recommended to use the PV or stratospheric tracer definitions when analyzing deep convection. The curvature of the BVF definition requires additional testing, and therefore is not recommended to be used in convective mass transport studies at this time. The WMO and static stability definitions are the best definitions to use when analyzing convective mass transport. However, because the WMO definition can easily be applied to any temperature profile in various regions of the globe without any alterations to criteria, it is the best tropopause definition for convective mass transport at this time. Additional studies should be performed on the static stability definition to determine criteria thresholds similar to that used in the WMO definition. At this time, the user must determine the static stability threshold from the pre–convective environment, making the definition difficult to apply to several case studies. This study highlights the importance of knowing which definitions are appropriate for deep convective studies. Since there are several definitions published in the literature, it is vital that we discuss their impact on mass transport as a scientific community. Studies that use differing definitions that do not provide similar results cannot be reliably compared. For

example, if one study uses the WMO definition while another uses the stratospheric tracer definition, those two studies cannot be compared to one another because the definitions provide vastly differing results. Additionally, many studies do not clearly state how tropopause definitions were calculated. Section 4.2.3.2 described the change in mass transport due to a simple calculation choice. Many definitions are often worded in a vague manner, making them open to the user's interpretation, such as the WMO thermal tropopause. It is important for studies to clearly communicate how they are calculating these definitions.

REFERENCES

Barber, K. (2015), Simulations of convectively–induced turbulence based on radar–based climatology of tropical storm types, *University of North Dakota thesis.*

Barber, K., G. Mullendore, and J. Alexander (2017), Impacts of model resolution and estimations method on convective–turbulence prediction, *In preparation.*

Bethan, S., G. Vaughan, S. J. Reid (1996), A comparison of ozone and thermal tropopause heights and the impact of tropopause definition on quantifying the ozone content of the troposphere, *Quarterly Journal of the Royal Meteorological Society,* **122**, 929–944.

Bigelbach, B. C. (2010), Exploring the differences in deep convective transport characteristics between quasi–isolated strong convection and mesoscale convective systems using seasonal WRF simulations, *University of North Dakota thesis.*

Birner, T. (2010), Residual circulation and tropopause structure, *Journal of Atmos. Sci.,* **76**, 2582–2600.

Dickerson, R. R., G. J. Huffman, W. T. Luke, L. J. Nunnermacker, K. E. Pickering, A. C. D. Leslie, C. G. Lindsey, W. G. N. Slinn, T. J. Kelly, P. H. Duam, A. C. Delany, J. P. Greenberd, P. R. Zimmerman, J. F. Boatman, J. D. Ray, D. H. Stedman (1987), Thunderstorms: An important mechanism in the transport of air pollutants, *Science,* **235**, 460–465.

Feichter, J. and P. J. Crutzen (2002), Parameterization of vertical tracer transport due to deep cumulus convection in a global transport model and its evaluation with [222]Radon measurements, *Tellus: Series B chemical and physical meteorology*, **42**, doi: 10.1034/j.1600-0889.1990.00011.x.

Fischer, H., M. de Reus, M. Traub, J. Williams, J. Lelieveld, J. de Gouw, C. Warneke, H. Schalger, A. Minikin, R. Scheele, P. Siegmund (2003), Deep convection injection of boundary layer air into the lowermost stratosphere at midlatitudes, *Atmospheric Chemistry and Physics: An interactive open access journal of the European Geosciences Union*, **3**,doi: 10.5194/acp-3-739-2003.

Fovell, R., D. Durran,and J. R. Holton (1992), Numerical simulations of convectively generated stratospheric gravity waves,*Journal of Atmospheric Sciences*, **49**, 1427–1442.

Frey, W., R. Schofield, P. Hoor, D. Kunkel, F. Ravegnani, A. Ulanovsky, S. Viciani, F. D'Amato, and T. P. Lane (2015), The impact of overshooting deep convection on local transport adn mixing in the tropical upper troposphere/lower stratosphere (UTLS), *Atmospheric Chemisty and Physics*, **15**, 6467–6486.

Fueglistaler, S., A. E. Dessler, T. J. Dunkerton, I. Folkins, Q. Fu, and P. W. Mote (2009), Tropical tropopause layer, *Review of Geophysics*, **47**, doi: 10.1029/2008RG000267.

Garcia, R. R. (1987), On the mean meridional circulation of the middle atmosphere, *Journal of the Atmospheric Sciences*, **44(24)**, 3599–3609.

Gettelman, A., and P. M. de F. Forster (2002), A climatology of the tropical tropopause layer, *Journal of the Meteorological Society of Japan*, **80**, 911–924.

Gettelman, A., P. Hoor, L. L. Pan, W. J. Randel, M. I. Hegglin, T. Birner (2011),The extratropical upper troposphere and lower stratosphere, 1–24.

Gray, S. L. (2003), A case study of stratosphere to troposphere transport: The role of convective transport and the sensitivity to model resolution, *Journal of Geophysical Research: Atmospheres*, **108**, doi: 10.1029/2002JD003317.

Hauf,T., P. Schulte, R. Alheit, and H. Schlager (1995), Rapid vertical trace gas transport by an isolated midlatitude thunderstorm, *Journal of Geophysical Research*, **100**, 22957-22970.

Hegglin, M. I., D. Brunner, H. Wernli, C. Schweirz, O. Martius, P. Hoor, H. Fischer, U. Parchatka, N. Spelten, C. Schiller, M. Krebsbach, U. Weers, J. Staehelin, Th. Peter (2004), Tracing troposphere–to–stratosphere transport above a mid–latitude deep convective system, *Atmospheric Chemsitry and Physics*, **4**, 741–756.

Highwood, E. J., and B. J. Hoskins (1998), The tropical tropopause, *Quarterly Journal of the Royal Meteorological Society*, **124**, 1579–1604, doi: 10.1002/qj.49712454911.

Hoerling, M. P., T. D. Schaack, A. J. Lenzen (1991), Global objective tropopause analysis, *Monthly Weather Review*, **119**, 1816–1831.

Hoinka, K. P. (1997), The tropopause: discovery, definition, and demarcation, *Meteorol. Zeitschrift*, **6**, 281–303.

Holton, J. R. (2013), An introduction to dynamic meteorology (fifth edition), *Academic Press*.

Homeyer, c. R., L. L. Pan, S. W. Dorsi, L. M. Avallone, A. J. Weinheimer, A. S. O'Brien, J. P. DiGangi, M. A. Zondlo, T. B. Ryerson, G. S. Diskin, and T. L.

Compos (2014), Convective transport of water vapor into the lower stratosphere observed during double–tropopause events, *Journal of Geophysical Research: Atmospheres*, **119**, 10941–10958, doi: 10.1002/2014JD021485.

Homeyer, C. R. (2015), Numerical simulations of extratropical tropopause–penetrating convection Sensitivities to grid resolution, *Journal of Geophysical Research: Atmospheres*, **120**, 7174–7188, doi: 10.1002/2015JD023356.

Kassner, C. (1909), Bericht uber die elfte allgemeine Versammlung und Feir des 25jakrigen Bestehens der Deutschen Meteorologischen Gesellschaft zu Hamburg am 28. bis 30. September 1908, *Meteorol. Zeitschrift*, **26**, 2–10.

Kim, J., and S.-W. Son (2012), Tropical cold–point tropopause: Climatology, seasonal cycle, and intraseasonal variability derived from COSMIC GPS radio occultation measurements, *American Meteorological Society Journal of Climate*, **25**, 5345–5360.

Kunz, A., P. Konopka, R. Muller, and L. L. Pan (2011), Dynamic tropopause based on isentropic potential vorticity gradients, *Journal of Geophysical Research*, **116**.

Lane, T. P., Michael J. Reeder, and Terry L. Clark (2001), Numerical Modeling of Gravity Wave Generation by Deep Tropical Convection, *Journal of Atmospheric Sciences*, **58**, 12491274.

Lin, Y.-L., R. D. Farley, and H. D. Orville (1983), Bulk parameterization of the snow field in a cloud model, *Journal of Applied Meteorology and Climatology*, **22**, 1065–1092.

Lin, Y.-L. (2010), Mesoscale dynamics, *Cambridge University Press*, 293–313.

Markowski, P. and Y. Richardson (2012), Mesoscale meteorology in the midlatitudes, *John Wiley and Sons Ltd.*, Chapter 8.

Miyazaki, K., S. Watanabe, Y. Kawatani, Y. tomikawa, M. Takahashi, and K. Sato (2010b), Transport and mixing in the extratropical tropopause region in a high–vertical–resolution GCM. Part I: Potential vorticity and heat budget analysis, *Journal of Atmospheric Sciences*, **67(5)**, 1293–1314.

Mullendore, G. L., D. R. Durran, and J. R. Holton (2005), Cross-tropopause tracer transport in midlatitude convection, *Journal of Geophysical Research*, **110**, doi:10.1029/2004JD005059.

Pan, L. L., W. J. Randel, B. L. Gary, M. J. Mahoney, and E. J. Hintsa (2004), Definitions and sharpness of the extratropical tropopause: a trace gas perspective, *J. Geophys. Res.*, **109**, D23103, doi: 10.1029/2004JD004982.

Pan, L. L., C. R. Homeyer, S. Honomichl, B. A. Ridley, M. Weisman, M. C. Barth, J. W. Hair, M. A. Fenn, C. Butler, G. S. Diskin, J. H. Crawford, T. B. Ryerson, I. Pollack, J Peischl, and H. Huntrieser (2014), Thunderstorms enhance tropospheric ozone by wrapping and shedding stratospheric air, *Geophysical Research Letters*, **41**, 7785–7790, doi: 10.1002/2014GL061921.

Piani, C., D. Durran, M. J. Alexander, and J. R. Holton (2000), A numerical study of three-dimensional gravity waves triggered by deep dropical convection and their role in the dynamics of the QBO, *Journal of the Atmospheric Sciences*, **57**, 3689–3701.

Plumb, R. A. (2007), Tracer interrelationships in the stratosphere, *Reviews of Geophysics*, **45**, doi: 10.1029/2005RG000179.

Poulida, O., R. R. Dickerson, and A. Heymsfield (1996), Stratosphere-troposphere exchange in a midlatitude mesoscale convective complex: 1. Observations, *Journal of Geophysical Research*, **101**, 6823–6836.

Randel, W. J., D. J. Seidel, L. L. Pan (2007), Obersvational characteristics of double tropopauses, *Journal of Geophysical Research*, **112**, doi: 10.1029/2006JD007904.

Randel, W. J., F. Wu (2007), The extratropical tropopause inversion layer: Global observations with GPS data, and a radiative forcing mechanism, *Journal of the Atmospheric Sciences*, **64**, 4489–4496, doi: 10.1175/2007JAS2412.1.

Santer, B. D., M. F. Wehner, T. M. L. Wigley, R. Sausen, G. A. Meehl, K. E. Taylor, C. Amman, J. Arblaster, W. M. Washington, J. S. Boyle, W. Bruggemann (2003), Contributions of anthropogenic and natural forcing to recent tropopause height changes, *Science*, **301**, 479–483.

Shepherd, T. G. (2007), Transport in the middle atmosphere, *Journal of the Meteorological Society of Japan*, **85**, 165–191.

Skamarock, W. C., J. G. Powers, M. Barth, J. E. Dye, T. Matejka, D. Bartels, K. Baumann, J. Stith, D. D. Parish, G. Hubler (2000), Numerical simulations of the July 10 stratospheric-tropospheric experiment: radiation, aerosols, and ozone/deep convection experiment convective system: kinematics and transport, *Journal of Geophysical Research*, **105**, 19973–19990.

Skamarock, W. C., J. B. Klemp, J. Dudhia, D. O. Gill, D. M. Barker, M. G. Duda, X-Y. Huang, W. Wang, J. G. Powers (2008), A description of the advanced research WRF version 3, *NCAR Technical Notes*

Tao, W. -K., and J. Simpson (1993), Goddard cumulus ensemble model. Part I: Model description, *Terr. Atmos. Oceanic. Sci.*, **4**, 35–72.

Towhy, C. H., C. F. Clement, B. W. Gandrud, A. J. Weinheimer, T. L. Campos, D. Baumgardner, W. H. Brune, I. Faloona, G. W. Sachse, S. A. Vay, D. Tan (2002),

Deep convection as a source of new particles in the midlatitude upper troposphere, *Journal of Geophysical Research*, **107**, doi:10.1029/2001JD000323.

Teisserenc de Bort, L. (1902), Variations de la tempèrature de l'air libre dans la zone comprise entre 8 km et 13 km d'altitude, Comptes rendus hebdomadaires des séances de l'Académie des sciences/publiés, **134**, 987–989.

Wallace, J. M., and P. V. Hobbs (1977), *Atmospheric Science: An introductory survey*, Academic Press, 68 pp.

Weisman, M. L., and J. B. Klemp (1982), The dependence of numerically simulated convective storms on vertical wind shear and buoyancy, *Journal of American Meteorological Society*, **110**, 504–520, doi:http://dx.doi.org/10.1175/1520-0493(1982)110¡0504:TDONSC¿2.0.CO;2.

World Meteorological Organization (1957), Definition of the tropopause, *World Meteorological Organization Bulletin*, **6**, 136.

Sahn, Z., C. A. M. Brenninkmeijer, and P. F. J. van Velthoven (2004), Passenger aircraft project CARIBIC 1997–2002, Part I: the extratropical chemical tropopause, *Atmos. Chem. Phys. Discuss.*, **4**, 1091–1117.